



Title	Analysis of the role of Src kinase in intraocular pressure elevation in glaucoma
Author(s)	塚本, 晃久
Citation	大阪大学, 2018, 博士論文
Version Type	VoR
URL	<a href="https://doi.org/10.18910/70720">https://doi.org/10.18910/70720</a>
rights	
Note	

*The University of Osaka Institutional Knowledge Archive : OUKA*

<https://ir.library.osaka-u.ac.jp/>

The University of Osaka

# Analysis of the role of Src kinase in intraocular pressure elevation in glaucoma

(緑内障の眼圧上昇における Src キナーゼの役割の解析)

A Doctoral Thesis

Teruhisa Tsukamoto

Department of Oncogene Research,  
Research Institute for Microbial Diseases,  
Osaka University

July 2018

## Contents

Abbreviations	5
Abstract	7
Introduction	8
Materials and methods	13
Reagents and antibodies	13
Cell culture	13
Plasmid and siRNA	14
RT-PCR and microarray analysis	14
Immunoblotting and immunoprecipitation	15
LC-MS/MS analysis	15
Immunocytochemistry	16
Animal experiments	16
Histological analysis	17
Cell adhesion assay	17
Migration assay	18
Gel contraction assay	18
Enzyme-linked immunosorbent assay (ELISA)	18
Statistical analyses	19
Results	20
Dasatinib, a potent Src family kinase inhibitor, suppressed the elevation of IOP induced by TGF- $\beta$ 2	20
Src is activated by TGF- $\beta$ 2 in trabecular meshwork cells	20
Src activity is involved in TGF- $\beta$ 2 signaling	21
Src activation is involved in TGF- $\beta$ 2-induced phenotypic changes in trabecular meshwork cells	21
Expression of tissue plasminogen activator is suppressed by Src activation	22
Upregulation of CasL leads to functional activation of Src	23
Src is involved in TGF- $\beta$ 2-induced deposition of extracellular matrix in the trabecular meshwork	24
Discussion	25
Figures	30
Figure 1. Structure of the retina and visual field	30
Figure 2. The differences between open-angle glaucoma and angle-closure glaucoma	31
Figure 3. Structure of the eye and aqueous humor dynamics	31
Figure 4. Regulation of Src family kinases	32

Figure 5.	Dasatinib, a potent Src family kinase inhibitor, suppresses IOP elevation induced by TGF- $\beta$ 2	32
Figure 6.	The response of trabecular meshwork cells to dexamethasone and TGF- $\beta$ 2	33
Figure 7.	Levels of active Src is increased after TGF- $\beta$ 2 treatment in trabecular meshwork cells	33
Figure 8.	Src is activated by TGF- $\beta$ 2 in trabecular meshwork cells	34
Figure 9.	Src activation is involved in TGF- $\beta$ 2-induced morphological changes in trabecular meshwork cells	34
Figure 10.	Src activity is involved in TGF- $\beta$ 2 signaling	35
Figure 11.	Src activation is involved in TGF- $\beta$ 2-induced phenotypic changes in trabecular meshwork cells	36
Figure 12.	Src signaling is activated by knockdown of CSK	36
Figure 13.	CSK knockdown induces similar morphological changes to those induced by TGF- $\beta$ 2.	37
Figure 14.	CSK knockdown induces similar phenotypic changes to those induced by TGF- $\beta$ 2	37
Figure 15.	The expression of ECM-related genes is altered by TGF- $\beta$ 2	38
Figure 16.	TGF- $\beta$ 2-induce downregulation of tissue plasminogen activator is inhibited by dasatinib	38
Figure 17.	CSK knockdown-induced downregulation of tPA production is restored by dasatinib	39
Figure 18.	An unknown 100 kDa phosphorylated protein upregulated by TGF- $\beta$ 2 is CasL	39
Figure 19.	CasL upregulation induced by TGF- $\beta$ 2 precedes Src activation	40
Figure 20.	Upregulation of CasL leads to activation of Src via a functional interaction in HepG2 cells	40
Figure 21.	Upregulation of CasL leads to functional activation of Src in trabecular meshwork cells	41
Figure 22.	CasL knockdown suppresses TGF- $\beta$ 2-induced upregulation of fibronectin in trabecular meshwork cells	41
Figure 23.	TGF- $\beta$ 2 induces the accumulation and secretion of fibronectin in trabecular meshwork cells	42
Figure 24.	Src is involved in TGF- $\beta$ 2-induced ECM deposition in the trabecular meshwork	42
Figure 25.	Hypothetical mechanism for TGF- $\beta$ 2-induced IOP elevation in glaucoma	43
Figure 26.	Expression of c-Abl in trabecular meshwork cells and HepG2 cells	44
Figure 27.	Effects of TGF- $\beta$ 2 on the phosphorylation of Fyn and Yes	44
Tables		45

Table 1.	Primer sequences for qRT-PCR	45
Table 2.	Representative ECM-related genes regulated by TGF- $\beta$ 2	45
Table 3.	List of representative proteins identified by LC-MS/MS analysis	46
Table 4.	List of ECM-related genes regulated by TGF- $\beta$ 2	47
Table 5.	Expression of Src family kinases in microarray analysis	59
References		60
Publication		67
Acknowledgements		68

## Abbreviations

CasL	Crk-associated substrate lymphocyte type
cDNA	Complementary deoxyribonucleic acid
c-KIT	KIT proto-oncogene receptor tyrosine kinase
COL4A1	Collagen type IV $\alpha$ 1
Csk	C-terminal Src kinase
DEX	Dexamethasone
DMEM	Dulbecco's modified Eagle's medium
D-PBS	Dulbecco phosphate-buffered saline
ECM	Extracellular matrix
ELISA	Enzyme-linked immunosorbent assay
EMT	Epithelial mesenchymal transition
EPHA2	EPH receptor A2
FAK	Focal adhesion kinase
FBS	Fetal bovine serum
GAPDH	Glyceraldehyde 3-phosphate dehydrogenase
HDAC	Histone deacetylase
HEF1	Human enhancer of filamentation 1
HRP	Horseradish peroxidase
IB	Immunoblotting
IgG	Immunoglobulin G
IHC	Immunohistochemistry
IOP	Intra ocular pressure
IP	Immunoprecipitation
JCT	Juxtacanalicular connective tissue
mRNA	Messenger ribonucleic acid
NEDD9	Developmentally down-regulated protein 9
NTG	Normal tension glaucoma
PDGFR $\beta$	Platelet derived growth factor receptor beta
POAG	Primary open angle glaucoma
PCR	Polymerase chain reaction
qRT-PCR	Quantitative reverse transcription polymerase chain reaction
RGC	Retinal ganglion cell
SFKs	Src family tyrosine kinases
TGF- $\beta$	Transforming growth factor- $\beta$
TIGR	Trabecular meshwork-induced glucocorticoid response

TBS-T Tris buffered saline with Tween-20  
tPA Tissue plasminogen activator

## Abstract

Glaucoma, a progressive and irreversible optic neuropathy, is one of the leading causes of vision impairment worldwide. Elevation of intraocular pressure (IOP) due to TGF- $\beta$ -induced dysfunction of the trabecular meshwork is a risk factor for glaucoma, but the underlying molecular mechanisms remain elusive. Here, I show that Src kinase is involved in TGF- $\beta$ -induced IOP elevation. I observed that dasatinib, a potent Src family kinase inhibitor, suppressed TGF- $\beta$ 2-induced IOP elevation in rat eyes. Mechanistic analyses in human trabecular meshwork cells showed that TGF- $\beta$ 2 activated Src signaling and concomitantly increased cytoskeletal remodeling, cell adhesion, and extracellular matrix (ECM) accumulation. Src was activated via TGF- $\beta$ 2-induced upregulation of the Src scaffolding protein CasL, which mediates the assembly of focal adhesions, cytoskeletal remodeling, and ECM deposition. Activation of Src suppressed the expression of tissue plasminogen activator, thereby attenuating ECM degradation. Furthermore, dasatinib ameliorated TGF- $\beta$ 2-induced changes in the contractile and adhesive characteristics of trabecular meshwork cells, and ECM deposition. These findings suggest that Src activity is involved in TGF- $\beta$ -induced IOP elevation and identify Src signaling as a potential therapeutic target in glaucoma.

## Introduction

Glaucoma, a progressive and irreversible optic neuropathy, is one of the leading causes of blindness worldwide (Bourne et al., 2018; Congdon et al., 2004; Yamada et al, 2010). A retinal ganglion cell (RGC) is a type of retinal neuron (Fig. 1A). The retinal nerve fiber layer is formed by RGC axons and the optic nerve, which is a bundle of retinal nerve fibers, connects to the brain (Fig. 1B). In glaucoma, apoptotic death of RGCs and damage of the optic nerve cause structural changes (retinal nerve fiber defects, thinning of ganglion cell layer, and optic nerve head cupping, etc.) in the retina and optic nerve. The visual field is impaired as optic nerve damage progresses and some glaucoma patients develop blindness. Simulation of visual field defects in glaucoma patients is shown in Fig. 1C. The number of glaucoma patients is increasing and people with blindness due to glaucoma will reach 11.2 million by 2020 worldwide (Quigley and Broman, 2006).

Although the pathogenesis of glaucoma is not well understood, elevated intraocular pressure (IOP) is a risk factor that contributes to progression of visual field defects. Consistent with this, reduction of IOP suppresses visual field defects (Garway-Heath et al., 2015; Heijl et al., 2002), and reduction of IOP is currently the only evidence-based treatment for glaucoma. The mechanical theory is proposed as a mechanism to explain visual field defects caused by elevated IOP. The mechanical theory suggests that elevated IOP compresses RGC axons, resulting in the obstruction of anterograde and retrograde axonal transport. Impaired axonal transport leads to depletion of factors to maintain RGC homeostasis such as brain derived neurotrophic factor and induces RGC death (Pease et al., 2000; Quigley et al., 2000). Since visual impairment due to glaucoma is irreversible, it is important to detect pathological signs of glaucoma at early stages. Once diagnosed with glaucoma, the patients require long term IOP-lowering therapy such as medicinal treatment, laser therapy, or surgery and the goal of glaucoma therapy is to maintain visual function. Several drugs to decrease IOP have been used for treatment of glaucoma. For instance, prostaglandin analogues,  $\beta$ -blockers, carbonic anhydrase

inhibitors,  $\alpha$ 2-adrenoceptor agonist, and rho kinase inhibitors are available for glaucoma therapy. Of these, prostaglandin analogues are frequently used as first-line due to their efficacy and fewer systemic side effects. Although  $\beta$ -blockers are also first line therapy, their efficacy is considered to be inferior to that of prostaglandin analogues. However, these approved drugs are not necessarily effective in all glaucoma patients. For example, a previous report showed that approximately 20% and 30% of patients were non-responder in treatment with latanoprost, (prostaglandin analogue) and timolol ( $\beta$ -blocker), respectively (Camras and Hedman, 2003). Furthermore, side effects related to mechanism of action restrict the clinical use of these drugs in certain cases. Conjunctival hyperemia and iris pigmentation are well-known side effects of prostaglandin analogues. Beta-blockers may induce systemic side effects such as bradycardia and bronchoconstriction. Therefore, new IOP-lowering drugs with novel mechanism of action are desired.

Glaucoma is classified into open-angle and angle-closure glaucoma (Fig. 2). The angle between iris and cornea is open in open-angle glaucoma. In contrast, the angle is usually blocked by iris in angle-closure glaucoma. Furthermore, both open-angle and angle-closure glaucoma are divided into primary and secondary glaucoma. Secondary glaucoma is the glaucoma caused by other eye disorders or medical treatment such as glucocorticoids. Primary open-angle glaucoma (POAG) is the most common form of glaucoma and accounts for approximately 75% of all glaucoma cases (Iwase et al., 2004; Quigley and Broman, 2006; Yamamoto et al., 2005). Normal tension glaucoma (NTG) is thought to be a type of open angle glaucoma in which damage occurs to the optic nerve in the normal range of IOP (lower than 21 mmHg). Although the pathogenesis of NTG is still unknown, lowering IOP is effective in NTG as well (Collaborative Normal-Tension Glaucoma Study Group, 1998).

IOP, a risk factor of glaucoma, is regulated by the balance between the production and drainage of aqueous humor. The aqueous humor is formed in the ciliary body and drained through the trabecular meshwork and the uveoscleral pathway (Fig. 3A). In humans, the aqueous humor is mainly drained through the trabecular meshwork, which is located in the iridocorneal angle, into Schlemm's

canal. Aqueous outflow via the trabecular meshwork outflow increases with the elevation of IOP (IOP-dependent outflow). IOP elevation is thought to be caused by elevated resistance to the outflow of aqueous humor due to dysfunction of the trabecular meshwork in POAG (Johnson, 2006; Roy Chowdhury et al., 2015). Extracellular matrix (ECM) is a non-cellular substance that fills extracellular space as a supportive framework. ECM is involved in various cellular responses such as proliferation, migration, differentiation, and phenotypic expression of cells by acting as a scaffold. ECM is also known as a mediator of signal transduction. ECM proteins such as fibronectin and collagen IV are enriched in the trabecular meshwork to maintain its function (Acott and Kelley, 2008). Deposition of abnormal ECM or modulation of cytoskeleton in the trabecular meshwork may be responsible for increased resistance to outflow (Lutjen-Drecoll et al., 1981; Read et al., 2007; Vranka et al., 2015). However, the molecular mechanisms responsible for increasing outflow resistance remain unclear.

Trabecular meshwork consists of three cell layers as shown in Fig. 3B. Resistance to outflow of aqueous humor is thought to be generated in inner wall of Schlemm's canal and juxtaganular connective tissue (JCT) consisted of cells and ECM (Ethier et al., 1986). In the normal trabecular meshwork, the outflow of the aqueous humor appear to be regulated by turnover of ECM in response to mechanical stretch of JCT induced by IOP elevation, resulting in maintaining IOP homeostasis (Bradley et al., 1998; Bradley et al., 2001). Therefore, dysregulation of trabecular meshwork cells may induce abnormal deposition of ECM, leading to IOP elevation. Contraction and relaxation of the trabecular meshwork is also thought to regulate IOP (Nakajima et al., 2005; Wiederholt et al., 2000). Moreover, the number of trabecular meshwork cells decreases in POAG patients and IOP homeostasis is lost by death of trabecular meshwork cells with treatment of saponin in an enucleated human anterior segment culture model (Abu-Hassan et al., 2015; Alvarado et al., 1984). These indicate that trabecular meshwork cells play crucial roles in regulation of outflow of aqueous humor and IOP.

Trabecular meshwork cells used in this study were isolated from the juxtaganular and corneoscleral regions of human eye. I obtained trabecular meshwork cells from ScienCell Research

Laboratories, since they were used in several studies concerned with glaucoma (Cavet et al., 2015; Kalouche et al., 2016; Inoue-Mochita et al., 2018; Matsuda et al., 2015; Tellios et al., 2017). Increased expression of myocilin, a secreted glycoprotein (previously known as TIGR), induced by glucocorticoids is a reliable marker for trabecular meshwork cells, because the response is not observed in other cells around the trabecular meshwork (Keller et al., 2018). Although exact function of myocilin remains unclear (Nguyen et al., 1998), it is considered as one of the causative genes for POAG due to significant mutations (3 - 5%) in adult POAG populations (Allingham et al., 2009).

Transforming growth factor- $\beta$  (TGF- $\beta$ ) is a multifunctional growth factor that regulates cell growth, differentiation, adhesion, migration, ECM production, epithelial–mesenchymal transition (EMT), and malignant progression. TGF- $\beta$  has three isoforms (TGF- $\beta$ 1,  $\beta$ 2, and  $\beta$ 3) that commonly bind to serine/threonine kinase receptors (type I and type II). Upon ligand binding, the activated type II receptor phosphorylates the GS domain of the type I receptor, which in turn activates downstream signaling pathways, such as Smad phosphorylation (Heldin et al., 1997; Itoh and ten Dijke, 2007). TGF- $\beta$  also regulates the function of trabecular meshwork cells (Wordinger et al., 2007; Yu et al., 2015), and its dysregulation is implicated in the etiology of POAG. For instance, the expression level of TGF- $\beta$ 2, but not TGF- $\beta$ 1 or TGF- $\beta$ 3, in aqueous humor is higher in POAG patients than in controls (Agarwal et al., 2015; Ochiai and Ochiai, 2002; Yoneda et al., 2007). In an enucleated human anterior segment culture model, treatment with TGF- $\beta$ 2 decreases the outflow of aqueous humor via the trabecular meshwork, suggesting that TGF- $\beta$ 2 plays an important role in the regulation of IOP (Gottanka et al., 2004). Moreover, IOP elevation induced by the injection of TGF- $\beta$ 2 into the rat eyes caused the death of retinal ganglion cells which are injured in glaucoma (Hill et al., 2015).

Src family kinases (SFKs) are non-receptor tyrosine kinases that were the first proto-oncogene products to be identified (Jove and Hanafusa, 1987). SFKs include c-Src, c-Yes, Fyn, c-Fgr, Lyn, Hck, Lck, and Blk. SFKs are expressed in various types of cells and functional redundancy among SFKs is known (Thomas and Brugge, 1997). SFKs regulate cellular functions such as

cytoskeleton remodeling, cell adhesion, and cell migration (Huveneers and Danen, 2009; Parsons and Parsons, 2004; Thomas and Brugge, 1997). Dysregulation of SFKs is associated with various diseases, including cancer and fibrosis (Massip Copiz and Santa Coloma, 2016; Wang and Zhuang, 2017; Yeatman, 2004). Consistent with this, dasatinib, a potent SFK inhibitor, is prescribed for treatment of acute lymphoblastic leukemia or chronic myeloid leukemia. SFK activity is strictly regulated by tyrosine phosphorylation at specific sites. In the resting state, Src is phosphorylated at Tyr529 (in human) (Brown and Cooper, 1996; Cooper et al., 1986) by C-terminal Src kinase (Csk) (Nada et al., 1991; Nada et al., 1993; Okada, 2012), causing it to adopt an inactive conformation. In response to stimulation by extracellular signals, such as ECMs and growth factors (Ha et al., 2008; Kaplan et al., 1995; Kypta et al., 1990), Src is activated via autophosphorylation at Tyr418 (in human) (Fig. 4). Src functions as a component of the focal adhesion complex, which connects extracellular ECM to actin fibers, by phosphorylating other components such as focal adhesion kinase (FAK) and paxillin (Harte et al., 1996; Schaller, 2001). Previous study revealed that Src was activated during TGF- $\beta$ -induced EMT and that its activation promoted mesenchymal features, e.g., cell adhesion, migration and ECM production, which are tightly associated with cancer malignancy (Komiya et al., 2016; Miyazono, 2009). In trabecular meshwork cells, TGF- $\beta$  can also promote cytoskeletal remodeling, cell adhesion, and ECM production (Wecker et al., 2013; Wordinger et al., 2007; Yu et al., 2015), similarly to epithelial cells. Therefore, I hypothesized that SFKs may contribute to TGF- $\beta$ 2-induced IOP elevation in POAG as well. In this study, I analyzed the role of SFKs in TGF- $\beta$  signaling in human primary trabecular meshwork cells, focusing on Src as a representative SFK. I show that Src is activated by TGF- $\beta$ 2, and that it may contribute to TGF- $\beta$ -induced IOP elevation by promoting the contractile and adhesive properties of trabecular meshwork cells, as well as ECM deposition.

## Materials and methods

### Reagents and antibodies

SD-208 and dexamethasone were purchased from Wako Pure Chemical Industries. Dasatinib was purchased from BioVision. TGF- $\beta$ 2 was purchased from Cell Signaling Technology. Rhodamine-conjugated phalloidin was purchased from Cytoskeleton. Primary antibodies used were rabbit anti-GAPDH (1:5000–1:10000; 3700S; Santa Cruz Biotechnology), rabbit anti-Fyn (1:1000; sc-16; Santa Cruz Biotechnology), mouse anti-phosphotyrosine (4G10; 1:2000–1:5000; 05-1050; Millipore), rabbit anti-CSK (1:000; 4980S; Cell Signaling Technology), rabbit anti-FAK (1:1000; 13009S; Cell Signaling Technology), rabbit anti-paxillin pY118 (1:1000; 2541S; Cell Signaling Technology), mouse anti-CasL (1:1000; 4044S; Cell Signaling Technology), rabbit anti-Src (1:1000; 2123S; Cell Signaling Technology), mouse anti-Src (1:1000; 2110S; Cell Signaling Technology), rabbit anti-Abl (1:1000; 2862S; Cell Signaling Technology), rabbit anti-Yes (1:1000; 3201S; Cell Signaling Technology), rabbit anti-FAK pY576 (1:10000; ab76244; Abcam), rabbit anti-N-Cadherin (1:5000; ab76011; Abcam), rabbit anti-paxillin (IB 1:5000, IHC 1:250; ab32084; Abcam), rabbit anti-fibronectin (1:250; ab45688; Abcam), and rabbit anti-Src pY418 (IB 1:2000–1:5000, IHC 1:50; 44-660G; Thermo Fisher Scientific). Horseradish peroxidase-conjugated anti-mouse or rabbit IgG secondary antibodies were purchased from Cell Signaling Technology or Jackson Immuno Research Laboratories. Alexa Fluor 488-conjugated anti-rabbit IgG antibodies were purchased from Thermo Fisher Scientific.

### Cell culture

Primary human trabecular meshwork cells (Lot No.3423) were purchased from ScienCell Research Laboratories. The HepG2 cell line was purchased from the American Type Culture Collection. Cells were cultured in Dulbecco's modified Eagle's medium (DMEM) supplemented with 10% fetal bovine

serum (FBS) at 37°C in a 5% CO<sub>2</sub> incubator; trabecular meshwork cells were cultured on poly-L-lysine-coated plates. For experiments, cells were treated with reagents diluted in serum-free DMEM.

### **Plasmid and siRNA**

cDNAs encoding Src and CasL were inserted into pCAG-Hyg (Wako Pure Chemical Industries) and pmaxCloning (Lonza), respectively. pmaxGFP was purchased from Lonza. Negative-control siRNA (No.1), CSK siRNA (#1: s3612, #2: s223346), and CasL siRNA (#1: s9428, #2: s9429) were purchased from Ambion. Plasmids and siRNAs were transfected into trabecular meshwork cells using Nucleofector 4D (Lonza) and the P5 Primary Cell 4D-Nucleofector X Kit (Lonza). Nucleofection was performed using program DY138 after plasmids (1 µg) or siRNAs (2 µM) were added to cells (5 × 10<sup>5</sup> cells/100 µL) resuspended in the solution provided in the kit. After nucleofection, DMEM containing 10% FBS was added to the nucleofected cells. The next day, medium was changed to DMEM without FBS. Plasmids were transfected into HepG2 cells using Lipofectamine 3000 (Thermo Fisher Scientific).

### **RT-PCR and microarray analysis**

Total RNA was prepared using ISOGEN with Spin Column (Nippon Gene) or RNeasy Mini Kit (QIAGEN). cDNA was synthesized from total RNA using the PrimeScript RT Reagent Kit (TaKaRa-Bio). Quantitative polymerase chain reaction was performed using SYBR Premix Ex Taq II (TaKaRa-Bio), the CFX-96 real time PCR detection system (Bio-Rad Laboratories), and primers listed in Table 1. For microarray analysis, two-color Agilent Array analysis (SurePrint G3 Human GE 8 × 60K Ver3.0) was carried out by TaKaRa-Bio. RNA from two samples in each group were mixed and used for microarray analyses.

### **Immunoblotting and immunoprecipitation**

Cells were washed with Dulbecco phosphate-buffered saline (D-PBS) and lysed with ODG buffer (50 mM Tris-HCl, pH 7.4, 150 mM NaCl, 1 mM EDTA, 1% NP-40, 5% glycerol, 2% n-octyl- $\beta$ -D-glucoside) with a protease inhibitor cocktail containing 1 mM 4-(2-Aminoethyl)benzenesulfonyl Fluoride Hydrochloride, 0.8  $\mu$ g/mL aprotinin, 15  $\mu$ M E-64, 20  $\mu$ M Leupeptin Hemisulfate, 50  $\mu$ M Pepstatin, and 10  $\mu$ M Pepstatin A (Nacalai Tesque) and a phosphatase inhibitor cocktail containing imidazole, tetra-sodium ethylenediaminetetraacetate, sodium orthovanadate,  $\beta$ -glycerophosphoric acid disodium salt, sodium (+)-tartrate dihydrate, sodium fluoride, and disodium molybdate (VI) dihydrate (undisclosed concentration, Nacalai Tesque). Immunoprecipitation was performed with the Dynabeads-Protein A or G Immunoprecipitation Kit (Thermo Fisher Scientific). Equal amounts of protein were subjected to sodium dodecyl sulfate polyacrylamide gel electrophoresis (SDS-PAGE) and transferred to polyvinylidene difluoride membrane using the iBlot2 System (Thermo Fisher Scientific). Membranes were incubated with primary antibodies after blocking with BSA, ECL Blocking agent (GE Healthcare), or Bullet Blocking One for Western Blotting (Nacalai Tesque). After washing with TBS-T (25 mM Tris, 0.15 M NaCl, 0.05% Tween-20, pH 7.5), membranes were incubated with HRP-conjugated secondary antibody, and then washed with TBS-T. After detection with phospho-specific antibodies, the same blots were stripped and reprobed with total antibodies. Antibodies were diluted in TBS-T. Signals visualized with ImmunoStar LD were recorded on an ImageQuant LAS 4000 (GE Healthcare), and band intensity was quantified using ImageQuant TL software (GE Healthcare). Representative immunoblotting images obtained from at least three independent experiments are shown.

### **LC-MS/MS analysis**

Lysates prepared from trabecular meshwork cells treated with TGF- $\beta$ 2 were immunoprecipitated using anti-phosphotyrosine antibody (4G10) and the Dynabeads-Protein G Immunoprecipitation Kit

(Thermo Fisher Scientific). Protein samples were separated by SDS-PAGE. After visualization by silver staining, proteins were excised from the gel fragments. Digested samples were analyzed by nanocapillary reversed-phase LC-MS/MS using a C18 column (φ75 mm) on a nano LC system coupled to an ESI-MS/MS (LTQ Orbitrap Velos, Thermo Fisher Scientific). Direct-injection data-dependent acquisition was performed using one MS channel for every three MS/MS channels and dynamic exclusion for selected ions. Proteins were identified by database searching using Mascot Daemon (Matrix Science).

### **Immunocytochemistry**

Cells were fixed with 10% formalin neutral buffer solution for 10 min at room temperature. After washing with TBS-T, samples were permeabilized with 0.03% digitonin for 15 min, and blocked with Blocking One (Nacalai Tesque) or Blocking One-P (Nacalai Tesque). Cells were incubated with primary antibodies overnight at 4°C, followed by incubation with Alexa Fluor 488-conjugated secondary antibody and rhodamine–phalloidin for 1 h at room temperature. Antibodies and phalloidin were diluted in TBS-T containing 5% Blocking One or Blocking One-P. Samples were mounted with 50% glycerol after washing with TBS-T. Images were taken on a BIORÉVO BZ-9000 fluorescence microscope (KEYENCE). Representative images obtained from at least three independent experiments are shown.

### **Animal experiments**

All procedures were performed in accordance with the approved standard Guidelines for Animal Care and Use of Otsuka Pharmaceutical Co. Ltd under approval of the Animal Experiment Committee of Otsuka Pharmaceutical Co. Ltd (approved number: 16-0431). Male Brown Norway rats (7–8 weeks old) were purchased from Charles River Laboratories, Japan. Rats were anesthetized with pentobarbital sodium (50 mg/kg, i.p.), and oxybuprocaine hydrochloride 0.4% (ocular instillation).

Test solutions (volume, 3.5  $\mu$ L; vehicle, 5.25 ng/eye TGF- $\beta$ 2, or 5.25 ng/eye TGF- $\beta$ 2 + 35 pmol/eye dasatinib) were injected into the anterior chamber with a 32G needle and Hamilton syringe, after injection of air to avoid leakage of the test solutions. Injection was performed twice a week until day 16. IOP was measured with a TonoLab tonometer (Icare) in the conscious state between 8:30AM and 11:00AM. Oxybuprocaine hydrochloride 0.4% was instilled to anesthetize the surface of the cornea before measurement of IOP. Values of IOP displayed as valid after six rebounds were recorded, and the average was used as the final value.

### **Histological analysis**

Rats were sacrificed by CO<sub>2</sub> inhalation after the final measurement of IOP. Eyes were enucleated and fixed in 10% formalin neutral buffer solution for 2 h. After a sucrose gradient (10%, 20%, 30%), halved eyes were frozen in in optimal cutting temperature (OCT) compound (Tissue-Tek). Cryosections (16  $\mu$ m) cut with the cryostat were blocked with Blocking One (Nacalai Tesque). Sections were incubated overnight with anti-fibronectin antibody at 4°C. After washing with TBS-T, the sections were incubated with Alexa Fluor 488-conjugated anti-rabbit IgG. After additional washing with TBS-T, samples were mounted with ProLong Gold Antifade Mountant with DAPI (Thermo Fisher Scientific). Images were taken using a BIOREVO BZ-9000 (KEYENCE) and merged into Z-stack images with a BZ-II analyzer (KEYENCE). For quantification of fibronectin, the percentage of the area above the threshold within the trabecular meshwork was calculated using ImageJ Fiji.

### **Cell adhesion assay**

Trabecular meshwork cells were incubated with serum-free DMEM with or without reagents for 48 h. The centrifuged cells were resuspended in serum-free DMEM after detachment with trypsin-EDTA. Cell suspensions (1  $\times$  10<sup>3</sup> cells/well) were plated on collagen type I-coated 96-well plates and

incubated for 60 min at 37°C. After removal of the medium and washing with D-PBS, the attached cells were quantified by CellTiter-Glo Luminescent Cell Viability Assay (Promega).

### **Migration assay**

Migration was assessed using the CytoSelect 96-Well Cell Migration Assay (Cell Biolabs). Trabecular meshwork cells treated with siRNA were incubated with serum-free DMEM for 24 h. After detachment with trypsin-EDTA, the cells were pelleted by centrifugation and resuspended in serum-free DMEM. Cell suspensions ( $1 \times 10^4$  cells) were applied to the upper chamber, and 3 ng/mL TGF- $\beta$ 2 was added to the lower chamber. Migratory cells were quantified after incubation for 8 h.

### **Gel contraction assay**

The Collagen Gel Culturing Kit (Nitta Gelatin) was used for the collagen gel contraction assay. Trabecular meshwork cells were trypsinized and resuspended in serum-free DMEM at  $1 \times 10^6$  cells/mL. Cell suspensions were added to a mixture of collagen solution, Solution C, and 10 $\times$  DMEM on ice (1:7:1:1). The mixture (0.5 mL) was loaded into a 24-well plate coated with 1% BSA, and incubated at 37°C for 1 h. Collagen gels were formed by incubation at 37°C for 90 min, and then 0.5 mL of serum-free DMEM, with or without reagents, was added to the gels. After 1 h incubation, the collagen gels were scraped off the walls of the wells with a spatula. Gel area was measured after incubation for 24 h. Images of gels were taken with a digital camera (EOS M3, Canon), and the area of gels was quantified with a BZ-II analyzer (KEYENCE).

### **Enzyme-linked immunosorbent assay (ELISA)**

Culture supernatants of trabecular meshwork cells were collected and the concentration of tPA or fibronectin in the supernatants was quantified using DuoSet ELISA (tPA: DY7449-05, fibronectin: DY1918-05; R&D Systems) or the Quantikine ELISA Kit (DTPA00; R&D Systems).

### **Statistical analyses**

The data are presented as mean  $\pm$  SEM. Statistical analyses of quantitative data were performed by using the t-test or Dunnett test. A P value of less than 0.05 was considered statistically significant.

## Results

### **Dasatinib, a potent Src family kinase inhibitor, suppressed the elevation of IOP induced by TGF-β2**

To evaluate the contribution of SFK activity to IOP elevation induced by TGF-β2, I first performed an *in vivo* experiment in rat eyes. Repeated injection of TGF-β2 into the anterior chamber of rat eyes induced elevation of IOP, which was determined using a TonoLab tonometer. Elevation of IOP by TGF-β2 was significantly suppressed by simultaneous injection of dasatinib, a potent SFK inhibitor (Fig. 5). These results suggest that SFK is involved in the elevation of IOP induced by TGF-β2.

### **Src is activated by TGF-β2 in trabecular meshwork cells**

To verify whether Src is involved in TGF-β-induced IOP elevation, I analyzed the effects of TGF-β2 on tyrosine kinase signaling in human primary trabecular meshwork cells. I first characterized trabecular meshwork cells used in this study by analysis of myocilin expression after treatment of dexamethasone, since the upregulation of myocilin by glucocorticoids is a reliable marker for trabecular meshwork cells. Treatment with dexamethasone dramatically induced expression of myocilin mRNA as reported previously (Nguyen et al., 1998) (Fig. 6A). Next, I investigated the effects of TGF-β2 using these trabecular meshwork cells. TGF-β2 treatment induced morphological changes, with cells converting from a rod-like shape to a more enlarged and spread morphology (Fig. 6B). Upregulation of N-cadherin, an EMT marker, was also observed after TGF-β2 treatment (Fig. 7A and 7B), indicating that these cells were sensitive to TGF-β2. These observations demonstrate that the cells used in this study had the typical features of trabecular meshwork cells.

Immunoblot analysis with anti-phosphotyrosine antibody revealed that the tyrosine phosphorylation levels of 125 kDa, 100 kDa, 68 kDa, and 60 kDa proteins increased after TGF-β2 treatment (Fig. 7A). Analysis with an antibody specific for the active form of Src (pTyr418) showed

that levels of active Src were significantly increased 48 h after TGF- $\beta$ 2 treatment (Fig. 7A and 7C). In addition, immunoprecipitation assays with anti-Src antibody confirmed that Src was indeed activated by TGF- $\beta$ 2 treatment in trabecular meshwork cells (Fig. 8).

### **Src activity is involved in TGF- $\beta$ 2 signaling**

I next investigated the contribution of Src activity to TGF- $\beta$ 2 signaling in trabecular meshwork cells. Immunofluorescence analysis revealed that TGF- $\beta$ 2 treatment induced morphological changes that were accompanied by the accumulation of paxillin, F-actin, and active Src (pY418) at focal adhesions. Treatment with dasatinib suppressed these morphological changes and the assembly of focal adhesions (Fig. 9). Furthermore, immunoblot analysis revealed that TGF- $\beta$ 2-induced tyrosine phosphorylation of cellular proteins including the 100 kDa protein (Fig. 10A), FAK, paxillin, and Src (Fig. 10B and 10C) was abolished by treatment with dasatinib or SD-208, an inhibitor of the TGF- $\beta$  receptor. These results demonstrate that Src activity is involved in TGF- $\beta$ 2 signaling via the TGF- $\beta$  receptor.

### **Src activation is involved in TGF- $\beta$ 2-induced phenotypic changes in trabecular meshwork cells**

I showed that TGF- $\beta$ 2 induced accumulation of active Src at focal adhesion sites, suggesting that TGF- $\beta$ 2 facilitates the ECM-cell adhesion via Src activation. To verify this in a quantitative manner, I performed cell adhesion assays on collagen type I. Cell adhesion was significantly promoted by TGF- $\beta$ 2, but inhibited by dasatinib and SD-208 (Fig. 11A). Because IOP is regulated by contraction and relaxation of the trabecular meshwork tissues, I also performed collagen gel contraction assays. TGF- $\beta$ 2 treatment increased the ability of trabecular meshwork cells to contract the collagen gel, and this effect was significantly inhibited by dasatinib (Fig. 11B). These results suggest that Src activity is involved in TGF- $\beta$ -induced phenotypic changes in trabecular meshwork cells.

To further confirm the role of Src in the regulation of the trabecular meshwork, I induced Src activation by knocking down CSK, a negative regulator of SFKs. CSK knockdown increased

phosphorylation of Src Y418 and FAK Y576 (Fig. 12), and caused paxillin and active Src to accumulate at focal adhesions, as observed in TGF- $\beta$ 2-treated cells (Fig. 13). Furthermore, cell adhesion and migration assays revealed that cell adhesion to collagen type I and cell migration induced by TGF- $\beta$ 2 were significantly promoted by CSK knockdown (Fig. 14). These results indicate that CSK knockdown leading to Src activation phenocopied the changes observed in TGF- $\beta$ 2-treated trabecular meshwork cells.

### **Expression of tissue plasminogen activator is suppressed by Src activation**

To explore IOP-related genes that are regulated by TGF- $\beta$ 2 or Src, I performed microarray analysis of trabecular meshwork cells treated with TGF- $\beta$ 2. Among the genes whose expression levels were significantly altered by TGF- $\beta$ 2, I focused my analysis on genes related to regulation of ECM (Table 2 and Table 4), which potentially play important roles in IOP elevation. To further dissect the contribution of Src activity to gene expression, I examined the effects of dasatinib on the expression of certain genes. Dasatinib did not appreciably influence TGF- $\beta$ 2-dependent upregulation of fibronectin, collagen type 4A1, integrin- $\beta$ 3 or TGF- $\beta$ 2, indicating that expression of these genes is not directly regulated by Src signaling (Fig. 15). By contrast, TGF- $\beta$ 2-dependent downregulation of tissue plasminogen activator (tPA) was inhibited by dasatinib (Fig. 15), suggesting that Src is directly involved in the regulation of tPA expression. Further analysis of tPA expression revealed that dasatinib upregulated tPA production, and TGF- $\beta$ 2-induced downregulation of tPA production was restored by dasatinib (Fig. 16). Likewise, CSK knockdown leading to Src activation decreased tPA production, whereas dasatinib restored tPA production (Fig. 17). These results demonstrate that TGF- $\beta$ 2-induced activation of Src contributes to downregulation of tPA, which plays a crucial role in the regulation of ECM homeostasis (Gerometta et al., 2013; Yang et al., 2005).

## Upregulation of CasL leads to functional activation of Src

In trabecular meshwork cells, I observed that TGF- $\beta$ 2 treatment promoted tyrosine phosphorylation of an unknown 100 kDa protein in parallel with phosphorylation of Src substrates, including FAK and paxillin (Fig. 7A, 10A, and 10B). These observations suggest that the 100 kDa protein could be functionally associated with Src signaling. To identify the protein, I performed immunoprecipitation with anti-phosphotyrosine antibody followed by LC-MS/MS analysis. Among several candidates (Table 3), I focused analysis on CasL (also designated as NEDD9 or HEF1), because CasL is an approximately 100 kDa protein that serves as a scaffold protein for Src and FAK (Izumchenko et al., 2009). Immunoprecipitation with anti-CasL antibody verified that the 100 kDa phosphoprotein was indeed CasL (Fig. 18).

Expression of CasL at the mRNA and protein levels was upregulated by TGF- $\beta$ 2 treatment (Fig. 19A). However, mRNA expression was not inhibited by dasatinib, suggesting that CasL upregulation precedes Src activation (Fig. 19B). To characterize the functional interaction between Src and CasL, I introduced Src and/or CasL into HepG2 cells in order to achieve efficient expression of both proteins. Co-immunoprecipitation assays revealed that overexpressed CasL interacted with overexpressed Src (Fig. 20A). Under these conditions, the activity of Src (pY418) was increased (Fig. 20B), suggesting that upregulation of CasL leads to activation of Src via a functional interaction, consistent with a previous report (Sima et al., 2013). To confirm the role of CasL in trabecular meshwork cells, I nucleofected the vector containing the CasL gene and CasL siRNA into trabecular meshwork cells. Overexpression of CasL induced the activation of endogenous Src (Fig. 21A and 21B) and the downregulation of tPA production (Fig. 21C). Conversely, CasL knockdown suppressed TGF- $\beta$ 2-induced upregulation of fibronectin (Fig. 22A and 22B). These results indicate that CasL upregulation leads to functional activation of Src in trabecular meshwork cells.

## **Src is involved in TGF- $\beta$ 2-induced deposition of extracellular matrix in the trabecular meshwork**

I explored the deposition of ECM induced by TGF- $\beta$ 2 in the trabecular meshwork. TGF- $\beta$ 2 induced the accumulation and secretion of fibronectin in trabecular meshwork cells (Fig. 23). To investigate the link between deposition of ECM and increased IOP (Fig. 5), I performed immunofluorescence analysis of rat eyes after repeated injection of TGF- $\beta$ 2 into the anterior chamber. Fibronectin deposition in the trabecular meshwork was increased by TGF- $\beta$ 2, but significantly attenuated by dasatinib (Fig. 24).

## Discussion

In this study, I investigated the molecular mechanism responsible for elevation of IOP in glaucoma by analyzing the phenotypic changes induced by TGF- $\beta$ 2 in trabecular meshwork cells. A hypothetical model for TGF- $\beta$ 2-induced IOP elevation in glaucoma is depicted in Fig. 25. In this model, stimulation with TGF- $\beta$ 2 induces upregulation of genes encoding ECM proteins, integrins, and CasL. CasL functions as an activating scaffold of Src, resulting in activation of focal adhesions and actin cytoskeleton. Activation of Src further suppresses the expression of tPA, which contributes to abnormal accumulation of ECM. The auto-upregulation of TGF- $\beta$  further potentiates these cellular events by forming a positive-feedback circuit. As a consequence, trabecular meshwork tissues are physically remodeled, thus developing resistance to outflow of aqueous humor. The resultant elevation of IOP then leads to the onset of POAG.

My *in vivo* study demonstrated that repeated injection of TGF- $\beta$ 2 increased IOP in rat eyes, consistent with the results of a previous report (Hill et al., 2015), and that dasatinib treatment attenuated the elevation of IOP induced by TGF- $\beta$ 2. I used dasatinib to inhibit Src activity in this study since it was assumed that the phenotype of single SFK knockdown or knockout could not be identified due to functional redundancy among SFKs. Dasatinib is a potent dual inhibitor of Src family kinases with an IC<sub>50</sub> in the subnanomolar range and Abl with an IC<sub>50</sub> in a few nanomolar range (Lee and Gautschi, 2006; Lombardo et al., 2004). However, Abl is expressed at a negligible level in trabecular meshwork cells (Fig. 26). Dasatinib also inhibits receptor tyrosine kinases such as c-KIT, PDGFR $\beta$ , and EPHA2 with an IC<sub>50</sub> in a dozen nanomolar range. Given the inhibitory activity, dasatinib is less likely to act on these receptor tyrosine kinases in this study although the possibility cannot be completely denied. Furthermore, PP2, another Src family kinase inhibitor, has been shown to decrease IOP in ocular normotensive rabbits (Kirihara et al., 2014). These suggest that the effect of dasatinib can be largely attributed to inhibition of Src family kinase. Dasatinib is known to inhibit c-Src, Lck,

c-Yes, and Fyn within Src family kinases. Meanwhile, microarray analysis showed that the expression of Lck was negligible, suggesting that dasatinib could inhibit c-Src, c-Yes, and Fyn in the trabecular meshwork (Table 5). Immunoprecipitation assay with anti-Src antibody showed that Src was phosphorylated by TGF- $\beta$ 2. Although I attempted to perform immunoprecipitation assay with anti-Fyn and anti-Yes antibodies in preliminary study, the apparent phosphorylation of Fyn and c-Yes by TGF- $\beta$ 2 treatment was not observed (Fig. 27). Taken together, these results support my conjecture that Src activity is involved in the regulation of IOP. However, it is impossible to completely rule out the possibility that dasatinib affects other kinases. Further investigation is required in order to clearly show that the reduction of IOP by dasatinib is only attribution to Src inhibition.

I used commercially available primary human trabecular meshwork cells in this study. The trabecular meshwork cells were used in several studies including the investigation of the cellular events induced by TGF- $\beta$ 2 (Inoue-Mochita et al., 2015). The trabecular meshwork cells were characterized by immunofluorescence with specific antibodies against  $\alpha$ -smooth muscle actin (negative) and fibronectin (positive) according to manufacturer's certificate of analysis. Furthermore, I confirmed that dexamethasone induced drastic upregulation of myocilin mRNA. These indicate that the cells used in this study possessed typical features of trabecular meshwork cells. In future experiments, the results obtained by using trabecular meshwork cells are to be verified in an *in vivo* study.

To determine the molecular mechanisms underlying Src-mediated elevation of IOP, I examined Src function in human trabecular meshwork cells. I observed that TGF- $\beta$ 2 induced functional activation of Src due to phosphorylation of Src Y418 and the accumulation of active Src (pY418) at focal adhesions, resulting in increased levels of actin fibers and focal adhesions in trabecular meshwork cells. Focal adhesions connect ECM and intracellular actin fiber via integrins, and the interaction between ECM and integrin induces formation of protein complexes containing Src, FAK, and paxillin at focal adhesions. Src plays key roles in the regulation of signal transduction from

focal adhesions (Playford and Schaller, 2004), and also promotes cytoskeleton remodeling, cell adhesion, and motility (Carragher and Frame, 2004; Matsuyama et al., 2016). Therefore, Src signaling is induced by the accumulation of active Src at focal adhesions even though Src is not highly phosphorylated. Indeed, TGF- $\beta$ 2-induced cellular events were inhibited by dasatinib, and, conversely, CSK knockdown leading to Src activation phenocopied the effects induced by TGF- $\beta$ 2. These results indicate that functional activation of Src is implicated in TGF- $\beta$ 2-induced cytoskeletal remodeling and focal adhesion formation in trabecular meshwork cells. I also observed that dasatinib inhibited TGF- $\beta$ 2-induced contraction of collagen gel in which the trabecular meshwork cells were embedded. Because contraction of the trabecular meshwork is thought to increase IOP (Nakajima et al., 2005; Wiederholt et al., 2000), it is likely that Src-mediated modulation of cytoskeleton is involved in the elevation of IOP.

Microarray and qRT-PCR analyses revealed that TGF- $\beta$ 2 induced expression of genes related to the focal adhesion complex, including integrin and ECMs. These changes were not inhibited by dasatinib, indicating that these genes are regulated upstream of Src. Thus, expression of components of focal adhesions is directly regulated by TGF- $\beta$  signaling, but subsequent activation of Src is involved in assembling and activating the focal adhesion complex, enabling it to exert its function. Interestingly, my data showed that TGF- $\beta$ 2 upregulated its own expression, suggesting that a positive-feedback circuit accelerates the functional activation of the trabecular meshwork.

The abnormal deposition of ECM is thought to be one of the main causes of reduced outflow aqueous humor (Lutjen-Drecoll et al., 1989; Vranka et al., 2015). tPA, which degrades ECM by activating plasminogen and matrix metalloproteinase (Haraguchi et al., 2001; Yang et al., 2005), is implicated in the elevation of IOP. tPA is downregulated by glucocorticoids, which is another risk factor for IOP elevation (Kersey and Broadway, 2006; Seftor et al., 1994), and injection of tPA into the anterior chamber or overexpression of tPA decreases IOP in animal models of glucocorticoid-induced ocular hypertension (Gerometta et al., 2013; Kumar et al., 2013). These observations suggest that tPA

plays a key role in ECM regulation in the trabecular meshwork, and that its downregulation is associated with IOP elevation. I found that tPA was downregulated by TGF- $\beta$ 2, as well as by CSK knockdown leading to Src activation, whereas dasatinib treatment restored tPA expression. These observations suggest that downregulation of tPA through Src activation contributes to ECM remodeling, leading to IOP elevation. Moreover, I showed that expression of tPA is regulated by Src at the transcriptional level. tPA expression is increased by inhibition of histone deacetylase (HDAC) in vascular endothelial cells, and HDAC3 is activated by Src (Larsson et al., 2012; Longworth and Laimins, 2006). These results raise the possibility that activated Src decreases expression of tPA via HDAC activation in the trabecular meshwork as well, although further analysis is required to verify this possibility.

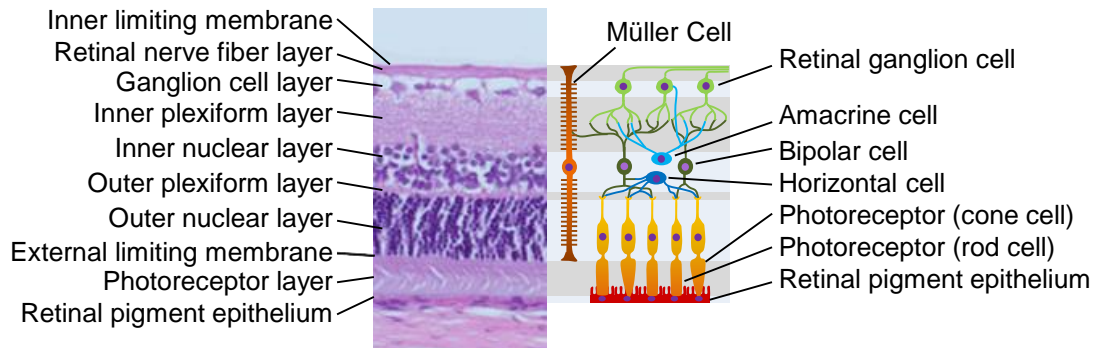
I found that a 100 kDa protein was phosphorylated on tyrosine by TGF- $\beta$ 2 treatment; LC-MS/MS analysis and immunoprecipitation assay identified this protein as CasL, an activating scaffold of FAK and Src (Izumchenko et al., 2009). I also observed that CasL expression was upregulated by TGF- $\beta$ 2, whereas dasatinib did not suppress CasL upregulation, indicating that CasL upregulation precedes Src activation. However, dasatinib inhibited phosphorylation of CasL, and overexpressed CasL interacted with and activated Src. These findings suggest that upregulated CasL interacts with Src to activate it, and that activated Src in turn phosphorylates CasL to create binding sites for additional signaling molecules, including Src and FAK. Thus, assembly of the signaling complex, i.e., the focal adhesion, is promoted. A similar interaction between CasL and Src was reported in HaCaT cells (Sima et al., 2013). Together, these findings suggest that a positive-feedback loop exists between Src and CasL in some cell types. Given that CasL is upregulated by TGF- $\beta$ 2 in the trabecular meshwork cells, it may act as a triggering molecule of Src-mediated signaling cascades associated with elevation of IOP in glaucoma. Although I focused my analysis on overexpression of CasL to identify the function as Src activator in trabecular meshwork cells in this study, further experiments are required to clarify the role of endogenous CasL in Src activation induced by TGF- $\beta$ 2.

Repeated injection of TGF- $\beta$ 2 increases IOP due to deposition of ECM in the trabecular meshwork (Hill et al., 2015). I showed that dasatinib treatment attenuated fibronectin deposition induced by TGF- $\beta$ 2 within the trabecular meshwork in rat eyes. The concentration of fibronectin in aqueous humor is higher in glaucoma patients than in controls (Kim et al., 1992), and the level of fibronectin in the trabecular meshwork increases with the pathological stage of glaucoma, as well as with aging (Babizhayev and Brodskaya, 1989). A recent report suggested that fibronectin fibrils were implicated in the assembly of ECM such as collagen IV and laminin by acting as a scaffold (Filla et al., 2017). These findings provide evidence for a functional link between fibronectin deposition and IOP. I found that TGF- $\beta$ 2 upregulated expression of fibronectin mRNA in trabecular meshwork cells, but was not inhibited by dasatinib. Nonetheless, dasatinib and CasL knockdown decreased deposition of fibronectin. This inconsistency could be explained by the upregulation of tPA production induced by dasatinib.

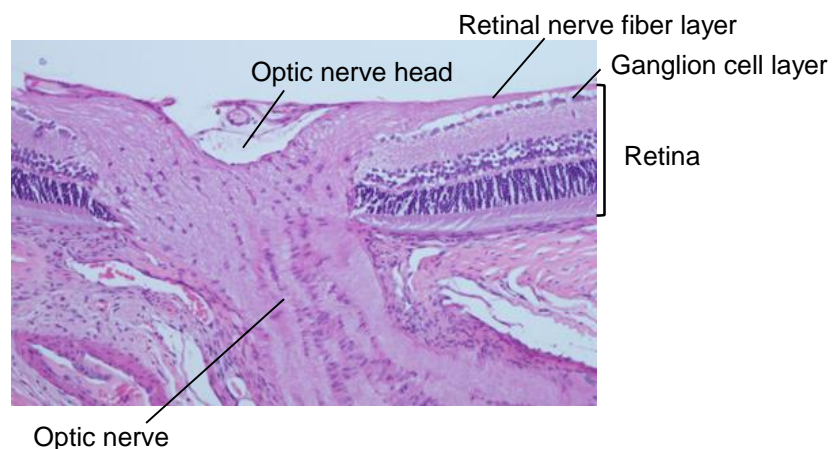
In summary, I demonstrated that the Src signaling pathway is involved in the elevation of IOP induced by TGF- $\beta$ 2, which plays a crucial role in POAG. Activated Src promotes remodeling of the trabecular meshwork via the upregulation of focal adhesions and ECM, and the downregulation of tPA, which is involved in ECM degradation. These Src-mediated cellular events may lead to IOP elevation by increasing resistance to aqueous humor outflow in trabecular meshwork tissues. These findings provide insights into the mechanisms underlying IOP elevation in glaucoma, and suggest that the Src signaling pathway represents a promising target for ocular hypotensive drugs for use against POAG.

## Figures

**A**



**B**



**C**



**Figure 1. Structure of the retina and visual field.** (A) Retina is composed of ten layers (left panel). The right panel shows the diagram illustrating retinal cells. (B) Hematoxylin and eosin-stained retinal histologic sections of rats. (C) Visual field simulation of a person with normal vision (left panel) and glaucoma (right panel).

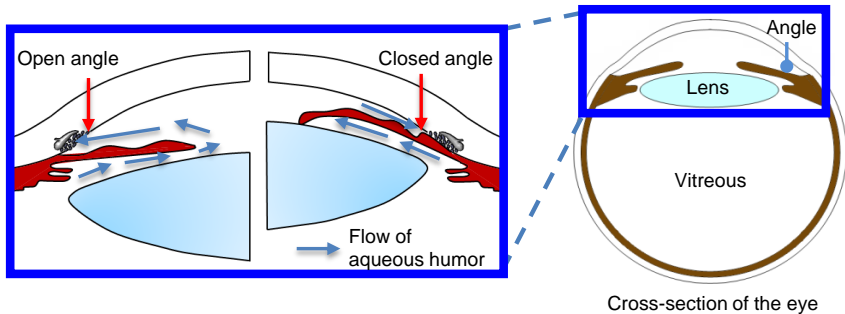
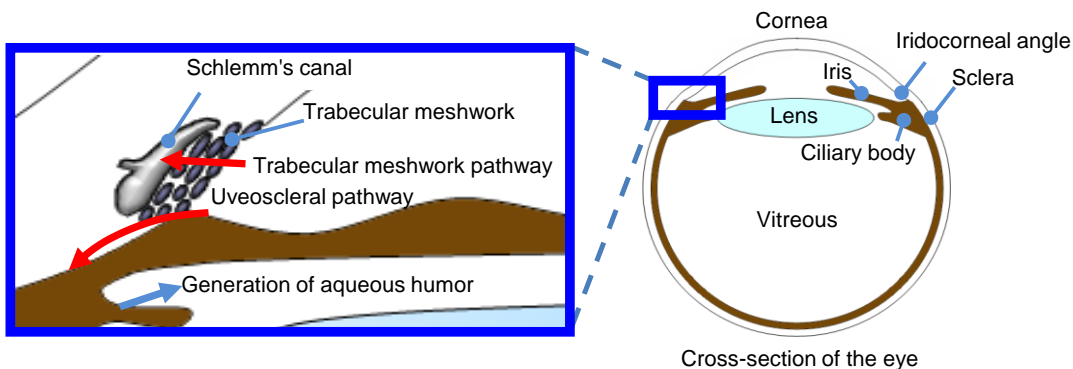


**Figure 2. The differences between open-angle glaucoma and angle-closure glaucoma.** Glaucoma is classified into open-angle and angle-closure glaucoma. The angle between iris and cornea is open in open-angle glaucoma. In contrast, the angle is usually blocked by iris in angle-closure glaucoma.

**A**



**B**

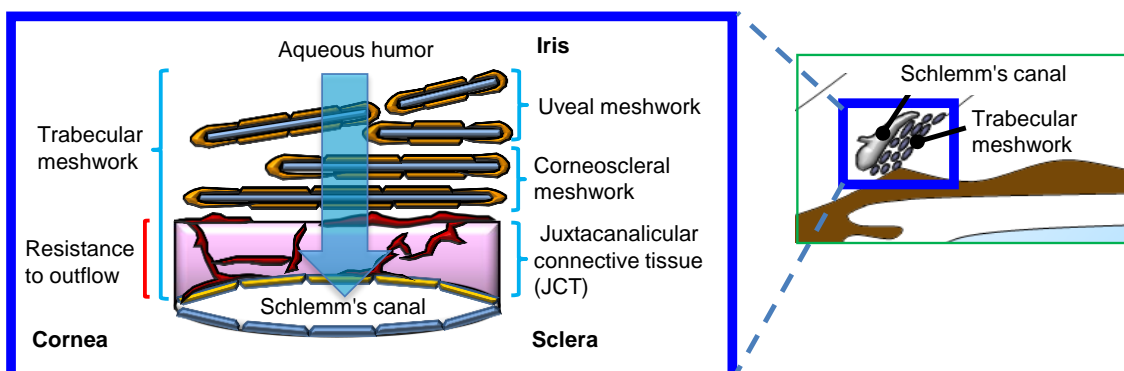


**Figure 3. Structure of the eye and aqueous humor dynamics.** (A) IOP is regulated by the balance between the production by the ciliary body and drainage of aqueous humor via trabecular meshwork and the uveoscleral pathway. In humans, the aqueous humor is drained mainly through the trabecular meshwork. (B) Trabecular meshwork consists of three cell layers (uveal meshwork, corneoscleral meshwork, and juxtacanalicular connective tissue (JCT)). Aqueous humor outflow resistance is generated in inner wall of Schlemm's canal and juxtacanalicular connective tissue (JCT) consisted of cells and ECM.

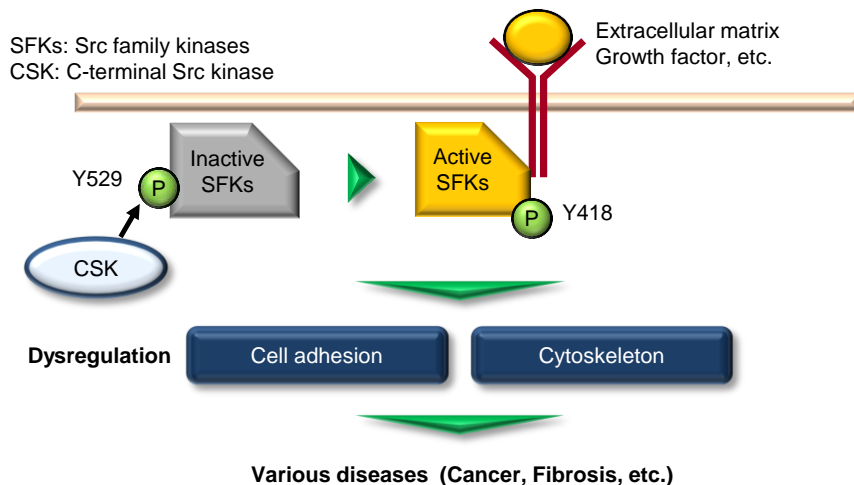


**Figure 4. Regulation of Src family kinases.** The activity of Src family kinases is strictly regulated by tyrosine phosphorylation at specific sites. In the resting state, Src is phosphorylated at Tyr529 by CSK, causing it to adopt an inactive conformation. In response to stimulation by extracellular signals, such as ECMs and growth factors, Src is activated via autophosphorylation at Tyr418. Dysregulation of SFKs is associated with various diseases, including cancer and fibrosis.

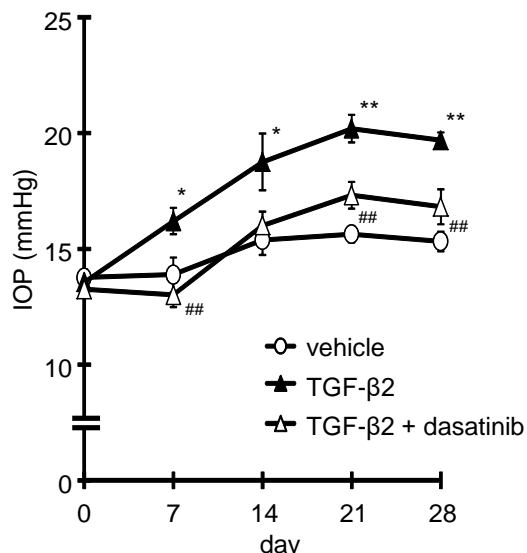


**Figure 5. Dasatinib, a potent Src family kinase inhibitor, suppresses IOP elevation induced by TGF- $\beta$ 2.** Vehicle and TGF- $\beta$ 2 (5.25 ng/eye) with or without dasatinib (35 pmol/eye) were injected into the anterior chamber of rats twice a week. IOP was measured (mean  $\pm$  SEM, n = 8) using TonoLab. \* P < 0.05, \*\* P < 0.01 vs. vehicle (unpaired t-test), ## P < 0.01 vs. TGF- $\beta$ 2 (unpaired t-test).

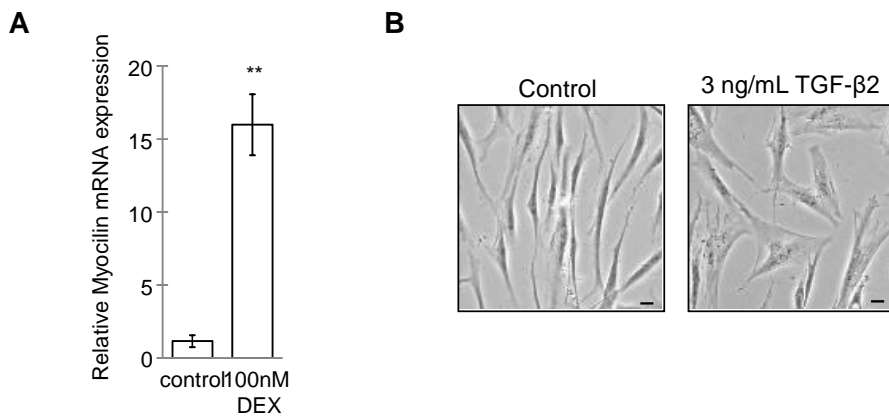


**Figure 6. The response of trabecular meshwork cells to dexamethasone and TGF- $\beta$ 2.** (A) qRT-PCR was performed on cells incubated for 72h with or without 100 nM dexamethasone (DEX) in serum-free DMEM. Data are presented as mean  $\pm$  SEM (n = 4). \*\* P < 0.01 vs. control (unpaired t-test). (B) Trabecular meshwork cells were treated for 48 h with or without 3 ng/mL TGF- $\beta$ 2 cells in serum-free DMEM. Cell morphology was observed by phase-contrast microscopy (IX71, OLYMPUS) at a magnification of  $\times 200$ . Scale bar = 20  $\mu$ m.

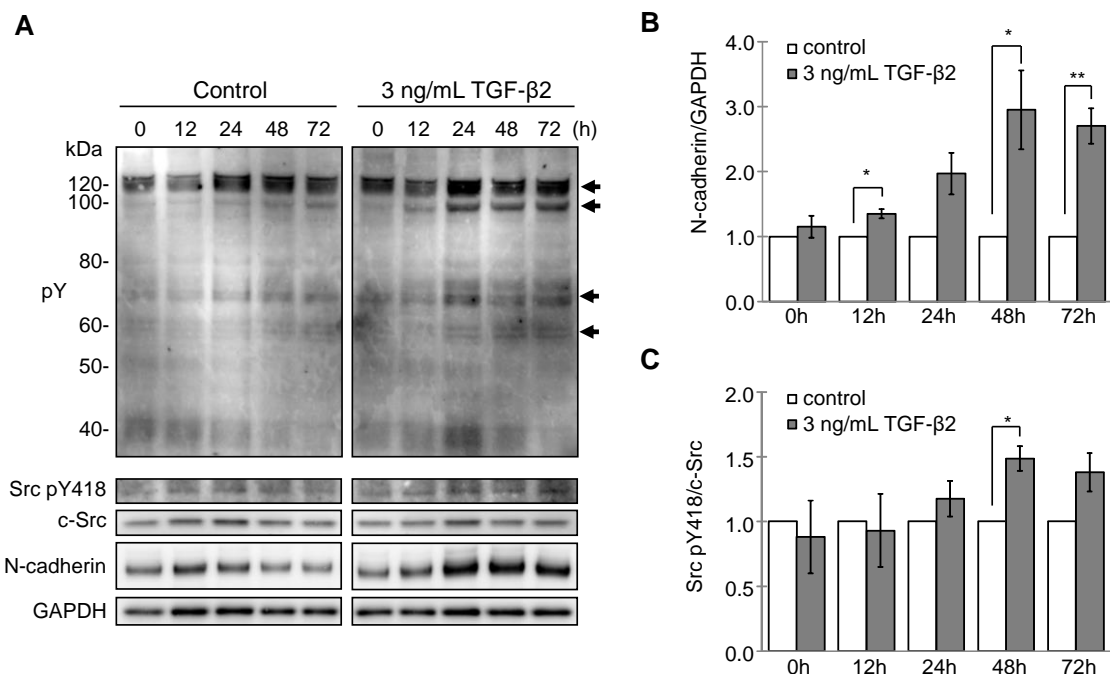


**Figure 7. Levels of active Src is increased after TGF- $\beta$ 2 treatment in trabecular meshwork cells.** (A) Trabecular meshwork cells were treated with 3 ng/mL TGF- $\beta$ 2 in serum-free DMEM. Immunoblotting was performed with the indicated antibodies. pY indicates anti-phosphotyrosine antibody (4G10). Arrows denote the locations of 125 kDa, 100 kDa, 68 kDa, and 60 kDa proteins. (B) The N-cadherin/GAPDH ratios are presented as mean  $\pm$  SEM (n = 4). \* P < 0.05 vs. control, \*\* P < 0.01 vs. control (unpaired t-test). (C) The Src pY418/c-Src ratios are presented as mean  $\pm$  SEM (n = 3) (lower graph). \* P < 0.05 vs. control (unpaired t-test).

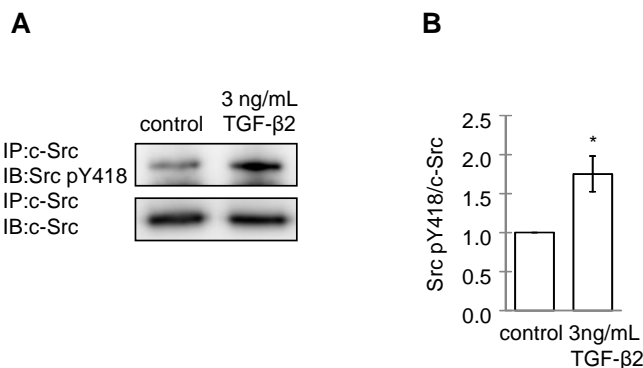


**Figure 8. Src is activated by TGF- $\beta$ 2 in trabecular meshwork cells.** (A) Anti-Src immunoprecipitates from cells treated with or without 3 ng/mL TGF- $\beta$ 2 for 48 h in serum-free DMEM were subjected to immunoblotting with anti-Src pY418 and anti-Src antibodies. (B) The Src pY418/c-Src ratios are presented as mean  $\pm$  SEM (n = 4). \* P < 0.05 vs. control (unpaired t-test).

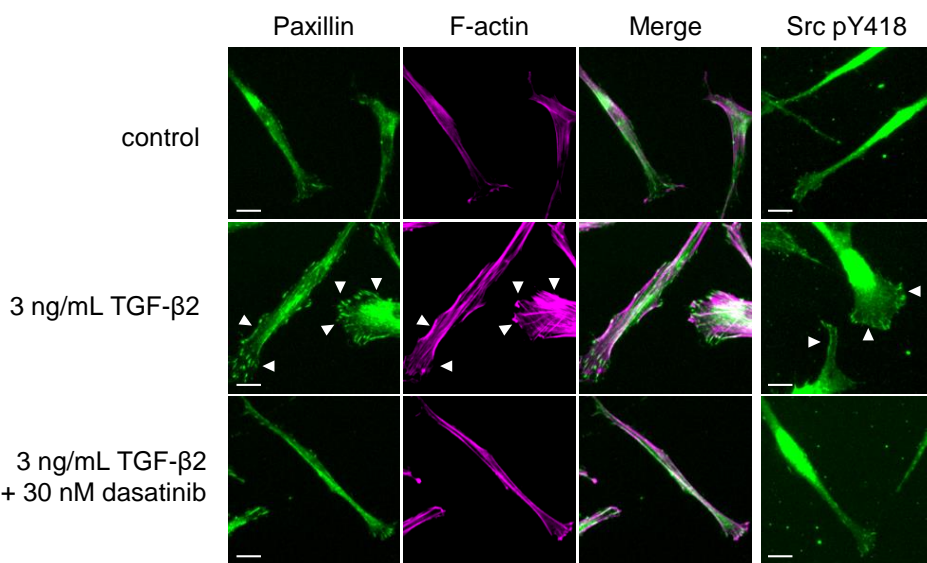


**Figure 9. Src activation is involved in TGF- $\beta$ 2-induced morphological changes in trabecular meshwork cells.**

Trabecular meshwork cells were incubated with serum-free DMEM containing the indicated reagents for 48 h. Cells immunostained with anti-paxillin, anti-Src pY418, and phalloidin were observed by fluorescence microscopy. Arrowheads indicate focal adhesion sites stained with anti-paxillin, F-actin, and anti-Src pY418. Scale bar = 20  $\mu$ m.

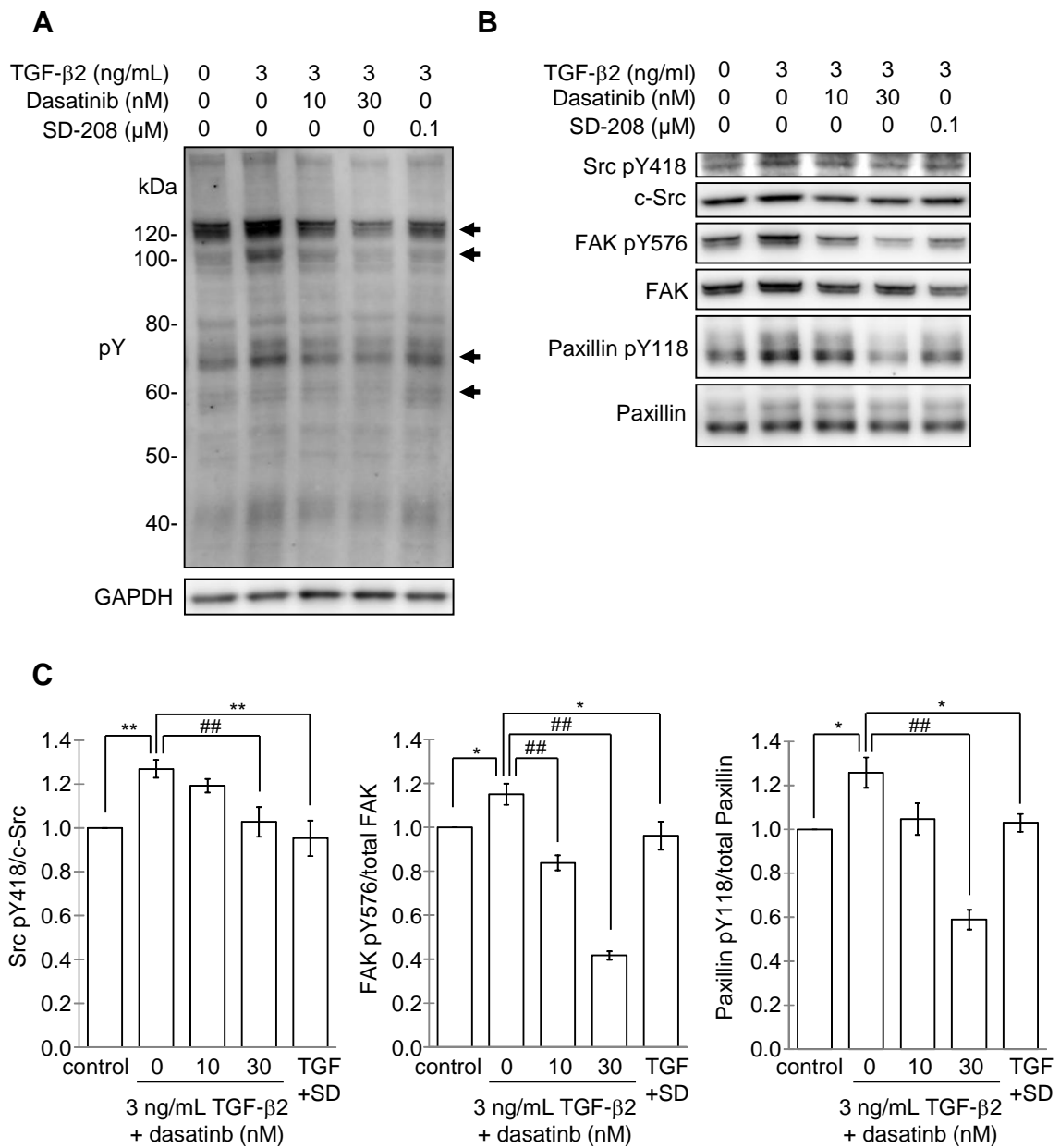


**Figure 10. Src activity is involved in TGF- $\beta$ 2 signaling.** Trabecular meshwork cells were incubated with serum-free DMEM containing the indicated reagents for 48 h. (A) Immunoblot with anti-phosphotyrosine antibody (pY: 4G10). Arrows denote the locations of 125 kDa, 100 kDa, 68 kDa, and 60 kDa proteins. (B) Immunoblots performed with the indicated antibodies are shown. (C) Src pY418/c-Src, FAK pY576/total FAK, and Paxillin pY118/total Paxillin ratios are presented as mean  $\pm$  SEM ( $n = 5$ ). \*  $P < 0.05$ , \*\*  $P < 0.01$  vs. control (unpaired t-test), ##  $P < 0.01$  vs. 3 ng/mL TGF- $\beta$ 2 (Dunnett test). TGF+SD indicates 3 ng/mL TGF- $\beta$ 2 plus 0.1  $\mu$ M SD-208.

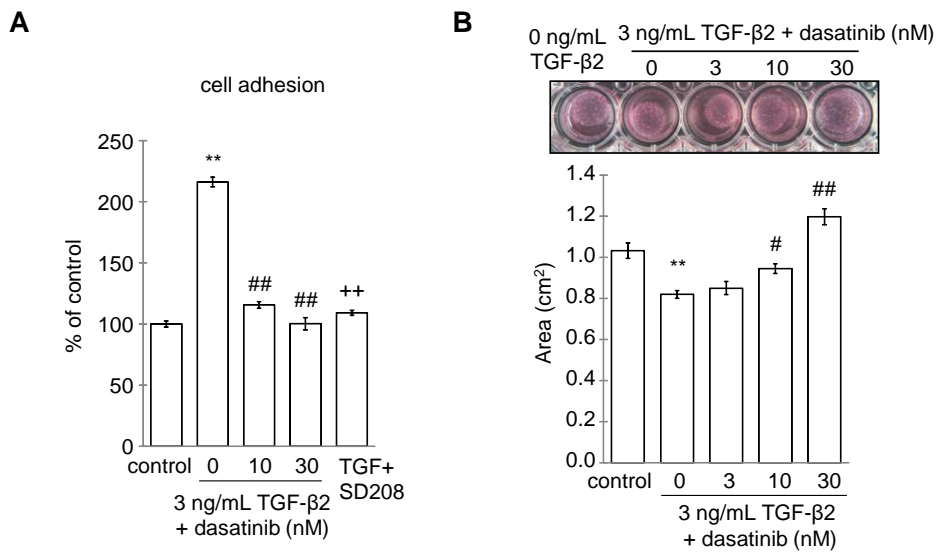


**Figure 11. Src activation is involved in TGF- $\beta$ 2-induced phenotypic changes in trabecular meshwork cells. (A)**

Trabecular meshwork cells were incubated with serum-free DMEM containing the indicated reagents for 48 h. Collected cells were plated in collagen type I-coated dishes and incubated with serum-free DMEM for 60 min. The number of cells was quantified by measurement of ATP (relative luminescence units: RLU) using the CellTiter-Glo Luminescent Cell Viability Assay Kit. The percentage of control was calculated (mean  $\pm$  SEM,  $n = 8$ ) by dividing the RLU of each group by that of the control group. TGF+SD indicates 3 ng/mL TGF- $\beta$ 2 plus 0.1  $\mu$ M SD-208. \*\*  $P < 0.01$  vs. control (unpaired t-test), ##  $P < 0.01$  vs. TGF- $\beta$ 2 + 0 nM dasatinib (Dunnett test), ++  $P < 0.01$  vs. TGF- $\beta$ 2 + 0 nM dasatinib (unpaired t-test). (B) Trabecular meshwork cells were embedded in collagen type I gels and incubated for 24 h with serum-free DMEM containing the indicated reagents. Images of gels were taken (upper panel), and gel area was quantified (mean  $\pm$  SEM,  $n = 4$ ). \*\*  $P < 0.01$  vs. control (unpaired t-test), #  $P < 0.05$ , ##  $P < 0.01$  vs. TGF- $\beta$ 2 + 0 nM dasatinib (Dunnett test) (lower panel).

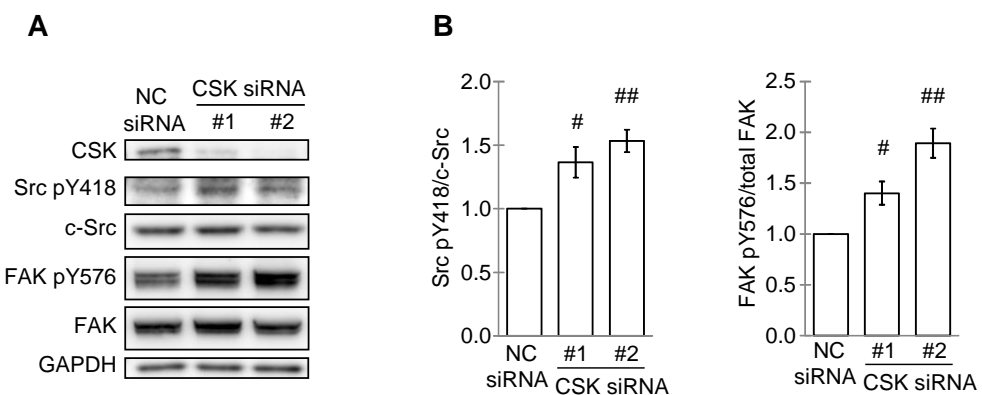


**Figure 12. Src signaling is activated by knockdown of CSK.** Trabecular meshwork cells were nucleofected with negative-control (NC) siRNA or CSK siRNA, followed by incubation with DMEM supplemented with 10% FBS for 24 h. #1 and #2 indicate CSK siRNA No.1 and No.2, respectively. (A) Immunoblotting was performed with the indicated antibodies. (B) Src pY418/c-Src and FAK pY576/total FAK ratios are presented as mean  $\pm$  SEM ( $n = 4$ ). #  $P < 0.05$ , ##  $P < 0.01$  vs. NC siRNA (Dunnett test).

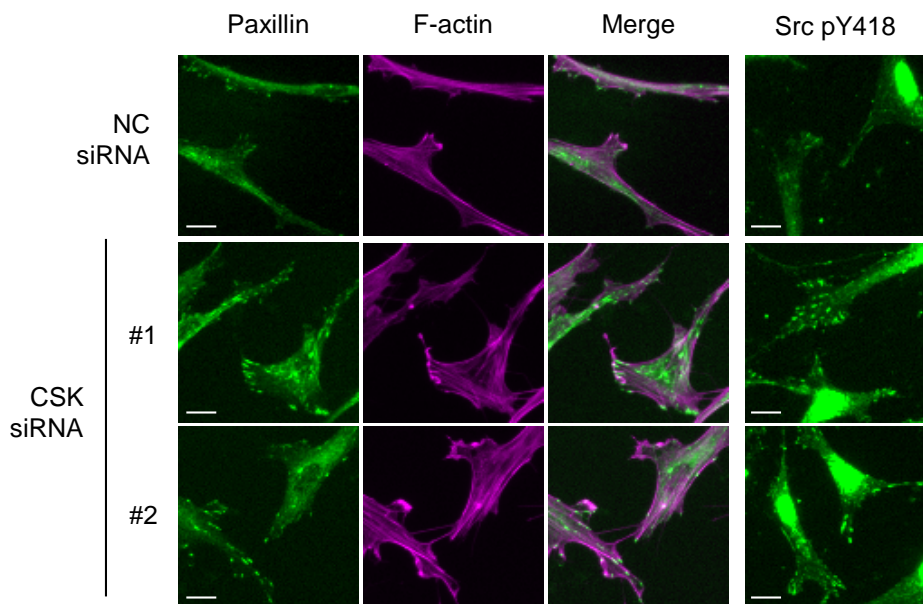


**Figure 13. CSK knockdown induces similar morphological changes to those induced by TGF- $\beta$ 2.** Trabecular meshwork cells were nucleofected with negative-control (NC) siRNA or CSK siRNA, followed by incubation with DMEM supplemented with 10% FBS for 24 h. #1 and #2 indicate CSK siRNA No.1 and No.2, respectively. Cells immunostained with anti-paxillin, anti-Src pY418, and phalloidin were observed by fluorescence microscopy. Scale bar = 20  $\mu$ m.

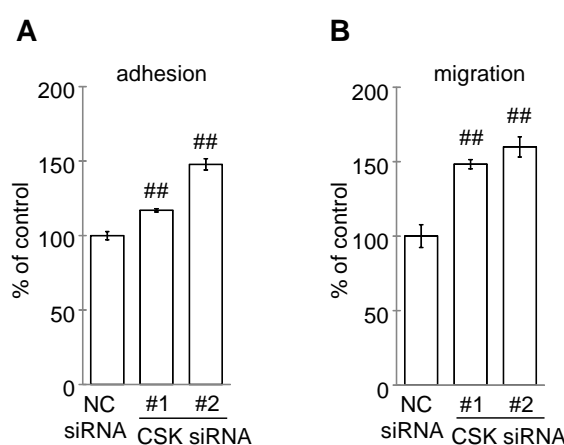


**Figure 14. CSK knockdown induces similar phenotypic changes to those induced by TGF- $\beta$ 2.** Trabecular meshwork cells were nucleofected with negative-control (NC) siRNA or CSK siRNA, followed by incubation with DMEM supplemented with 10% FBS for 24 h. Cells were incubated for 24 h (migration assay) or 48 h (others) after medium was replaced with serum-free DMEM. #1 and #2 indicate CSK siRNA No.1 and No.2, respectively. (A) Adhesion assay was performed as described in Figure 11A. (B) Migration assay. Percentage of control was calculated by dividing the RLU (adhesion assay, mean  $\pm$  SEM,  $n = 5$ ) or RFU (relative fluorescence units, migration assay, mean  $\pm$  SEM,  $n = 8$ ) of each group by that of the NC siRNA group. ##  $P < 0.01$  vs. NC siRNA (Dunnett test).

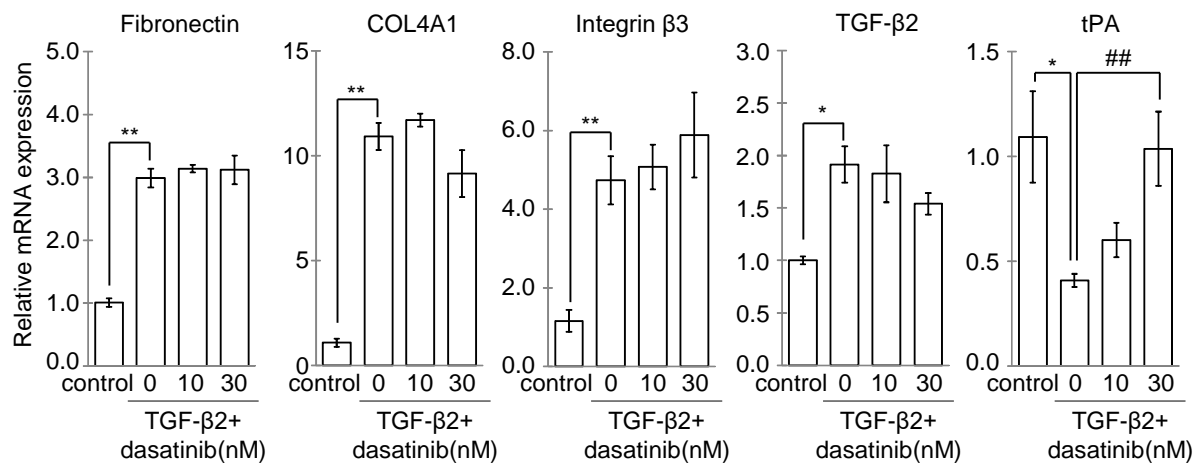


**Figure 15. The expression of ECM-related genes is altered by TGF-β2.** qRT-PCR was performed on cells incubated for 24 h with serum-free DMEM containing the indicated reagents. Data are presented as mean  $\pm$  SEM ( $n = 4$ ). \*  $P < 0.05$ , \*\*  $P < 0.01$  vs. control (unpaired t-test), ##  $P < 0.01$  vs. TGF-β2 + 0 nM dasatinib (Dunnett test).

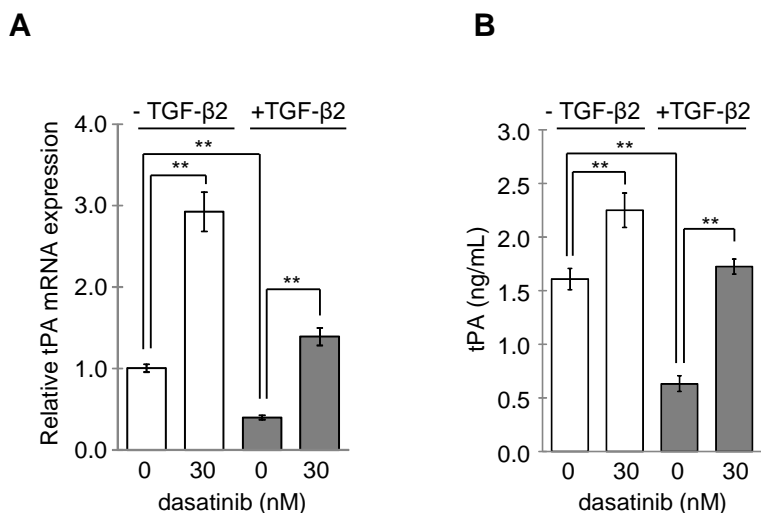


**Figure 16. TGF-β2-induce downregulation of tissue plasminogen activator is inhibited by dasatinib.** Cells were treated for 24 h with serum-free DMEM containing the indicated reagents, and (A) qRT-PCR (mean  $\pm$  SEM,  $n = 4$ ) was performed (left panel). (B) ELISA for tPA (mean  $\pm$  SEM,  $n = 7$ ) was performed on culture supernatants following incubation. \*\*  $P < 0.01$  (unpaired t-test).

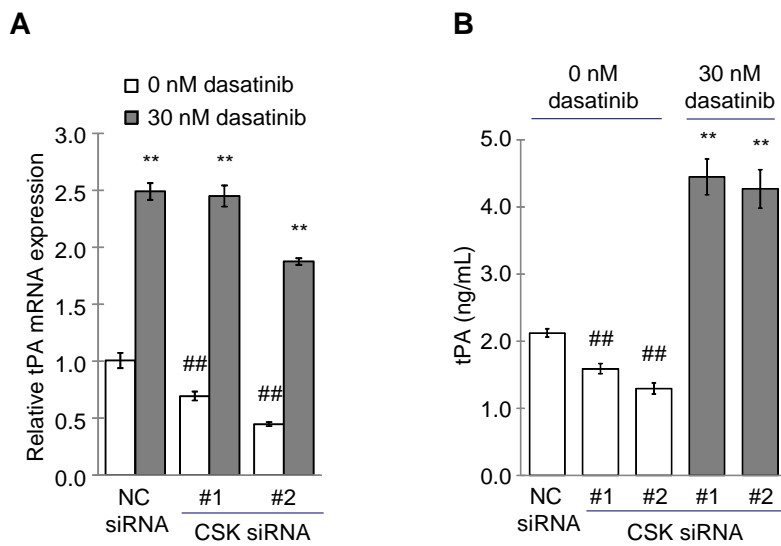


**Figure 17. CSK knockdown-induced downregulation of tPA production is restored by dasatinib.** Cells were nucleofected with negative-control (NC) siRNA or CSK siRNA, followed by incubation with DMEM supplemented with 10% FBS for 24 h. Cells were incubated for 48 h after medium was replaced with serum-free DMEM containing the indicated reagents, and (A) qRT-PCR (mean  $\pm$  SEM, n = 4) was performed (left panel). (B) ELISA for tPA (mean  $\pm$  SEM, n = 6) was performed on culture supernatants following incubation. #1 and #2 indicate CSK siRNA No.1 and No.2, respectively. ## P < 0.01 vs. NC siRNA (Dunnett test), \*\* P < 0.01 vs. NC siRNA, CSK siRNA No.1, or CSK siRNA No.2 (unpaired t-test).

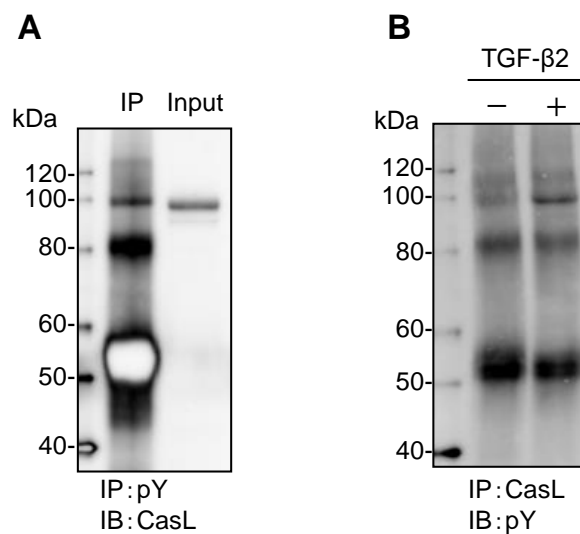


**Figure 18. An unknown 100 kDa phosphorylated protein upregulated by TGF- $\beta$ 2 is CasL.** (A) Total cell lysates and anti-phosphotyrosine antibody (pY: 4G10) immunoprecipitates from trabecular meshwork cells treated with TGF- $\beta$ 2 were immunoblotted with anti-CasL antibody (B) anti-CasL immunoprecipitates from trabecular meshwork cells treated with or without TGF- $\beta$ 2 were immunoblotted with anti-pY antibody.

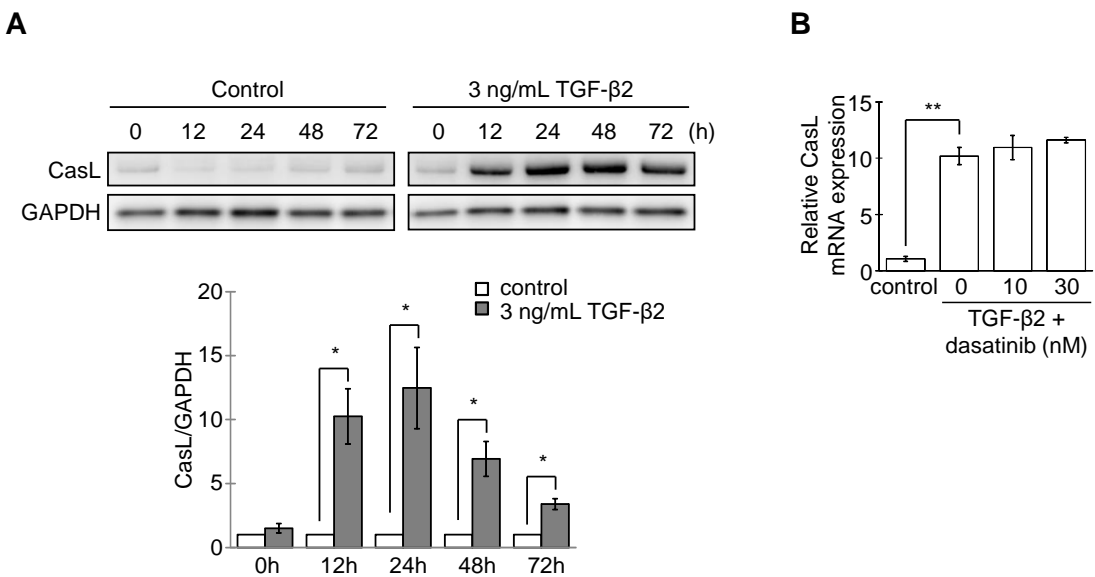


**Figure 19. CasL upregulation induced by TGF- $\beta$ 2 precedes Src activation.** Trabecular meshwork cells were treated with or without 3 ng/mL TGF- $\beta$ 2 in serum-free DMEM. **(A)** Lysates were subjected to immunoblotting with anti-CasL antibody (upper panel). The CasL/GAPDH ratios are presented as mean  $\pm$  SEM (n = 4) (lower panel). \* P < 0.05 vs. control (unpaired t-test). **(B)** qRT-PCR (mean  $\pm$  SEM, n = 4) was performed on trabecular meshwork cells treated for 24 h with the indicated reagents (lower panel). \*\* P < 0.01 vs. control (unpaired t-test).

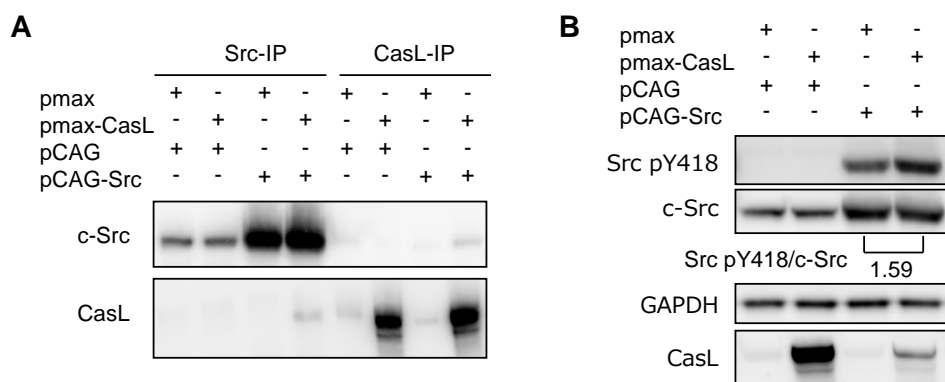


**Figure 20. Upregulation of CasL leads to activation of Src via a functional interaction in HepG2 cells.** (A) HepG2 cells were transfected for 24 h with the indicated constructs in DMEM supplemented with 10% FBS. After incubation with serum-free DMEM for 24 h, total cell lysates were prepared and immunoprecipitations were performed with the indicated antibodies. Subsequently, the immunoprecipitates were immunoblotted with the indicated antibodies. (B) Total cell lysates were immunoblotted with the indicated antibodies. The Src pY418/c-Src ratios are presented as averages (n = 3).

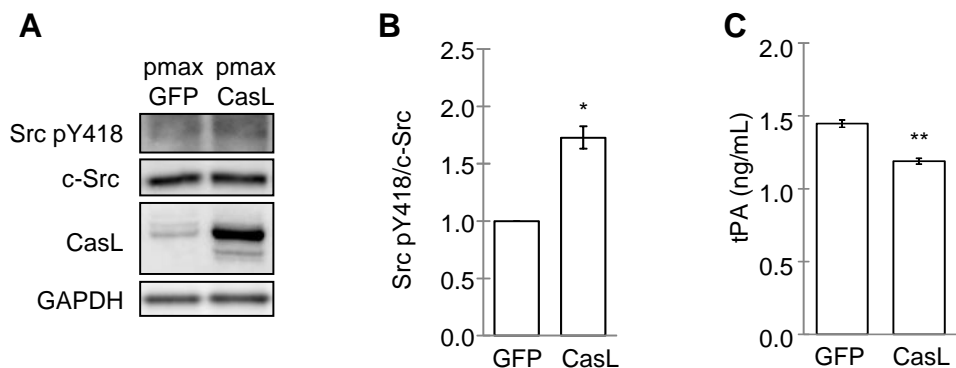


**Figure 21. Upregulation of CasL leads to functional activation of Src in trabecular meshwork cells.** (A) Trabecular meshwork cells nucleofected with the indicated constructs were incubated for 24 h with DMEM supplemented with 10% FBS, followed by incubation with serum-free DMEM for 24 h. Total cell lysates were immunoblotted with the indicated antibodies. (B) The Src pY418/c-Src ratios are presented as mean  $\pm$  SEM (n = 3). \* P < 0.05 vs. pmaxGFP (unpaired t-test). (C) Supernatants of the above cultures were subjected to tPA ELISA (mean  $\pm$  SEM, n = 6). \*\* P < 0.01 vs. pmaxGFP (unpaired t-test).

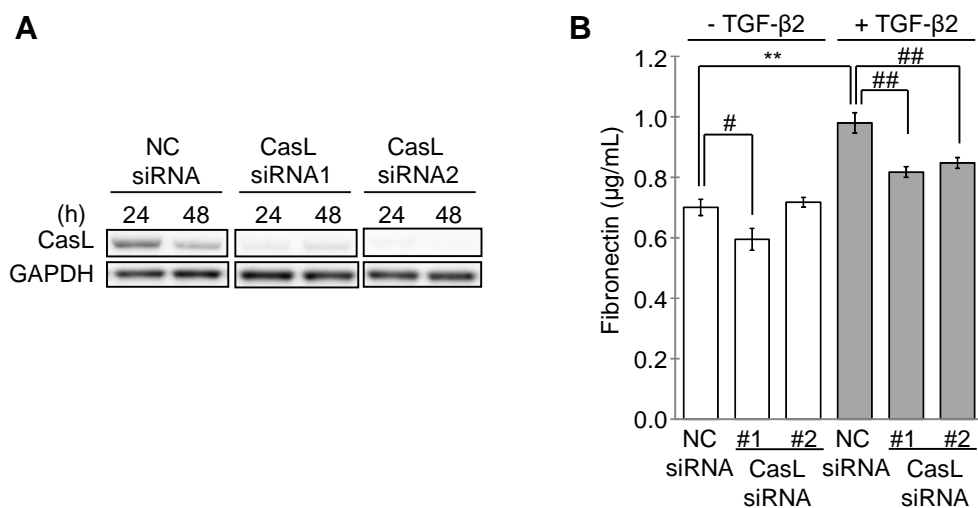


**Figure 22. CasL knockdown suppresses TGF- $\beta$ 2-induced upregulation of fibronectin in trabecular meshwork cells.** (A) Trabecular meshwork cells nucleofected with the indicated siRNAs were incubated for 24 h with DMEM supplemented with 10% FBS, followed by incubation with serum-free DMEM. Total cell lysates were immunoblotted with the indicated antibodies. (B) After incubation, culture supernatants were subjected to fibronectin ELISA (mean  $\pm$  SEM, n = 4). \*\* P < 0.01 (unpaired t-test), # P < 0.05, ## P < 0.01 (Dunnett test) (lower panel). #1 and #2 indicate CasL siRNA No.1 and No.2, respectively.

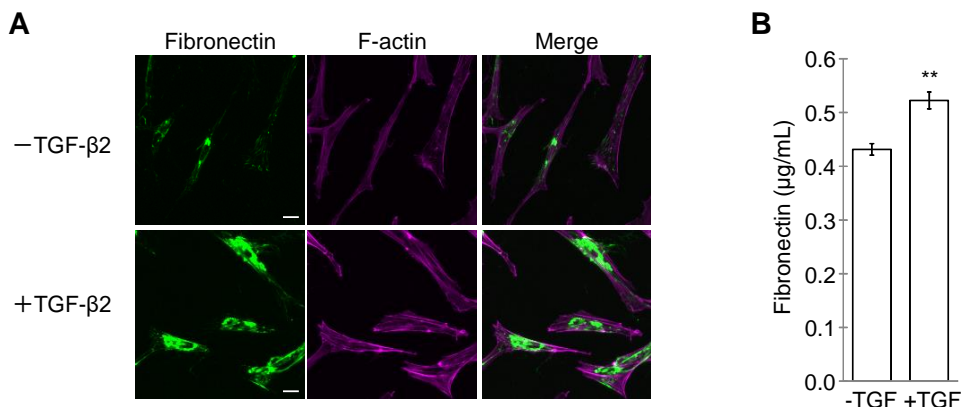


**Figure 23. TGF- $\beta$ 2 induces the accumulation and secretion of fibronectin in trabecular meshwork cells.** (A) Trabecular meshwork cells were incubated with or without 3 ng/mL TGF- $\beta$ 2 in serum-free DMEM for 24 h (fibronectin ELISA) or 48 h (immunostaining). Cells immunostained with anti-fibronectin and phalloidin were observed by fluorescence microscopy (left panels). Scale bar = 20  $\mu$ m. (B) Supernatants after incubation were subjected to fibronectin ELISA (mean  $\pm$  SEM, n = 8). \*\*P < 0.01 (unpaired t-test).

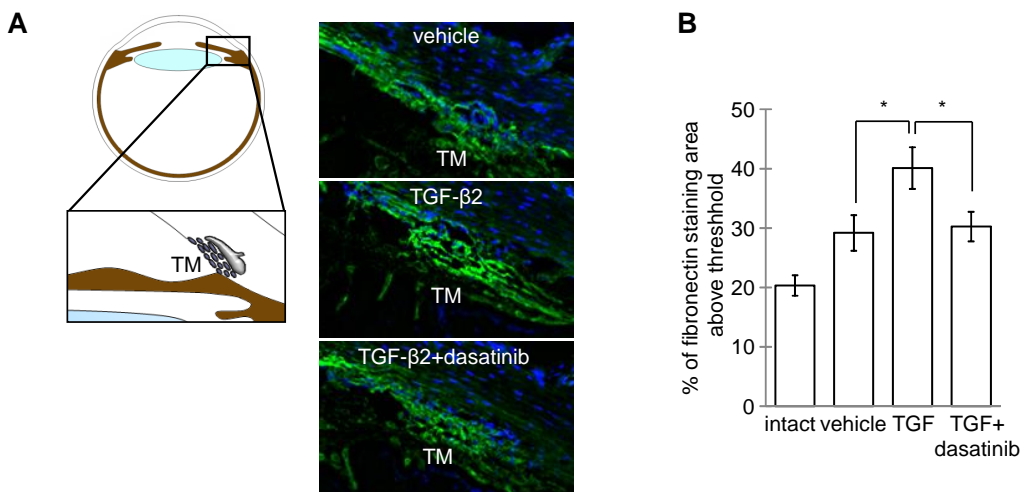


**Figure 24. Src is involved in TGF- $\beta$ 2-induced ECM deposition in the trabecular meshwork.** (A) The diagram illustrates the cross-section of the eye and the magnified view around the trabecular meshwork. TM indicates trabecular meshwork (left panel). After the last measurement of IOP, rat eyes were immunostained with anti-fibronectin (green). Blue immunofluorescent staining indicates nuclear staining with 4',6-diamidino-2-phenylindole (DAPI) (middle panels). Scale bar = 20  $\mu$ m. (B) Fibronectin within trabecular meshwork was quantified (mean  $\pm$  SEM, n = 7–8). \*P < 0.05 (unpaired t-test).

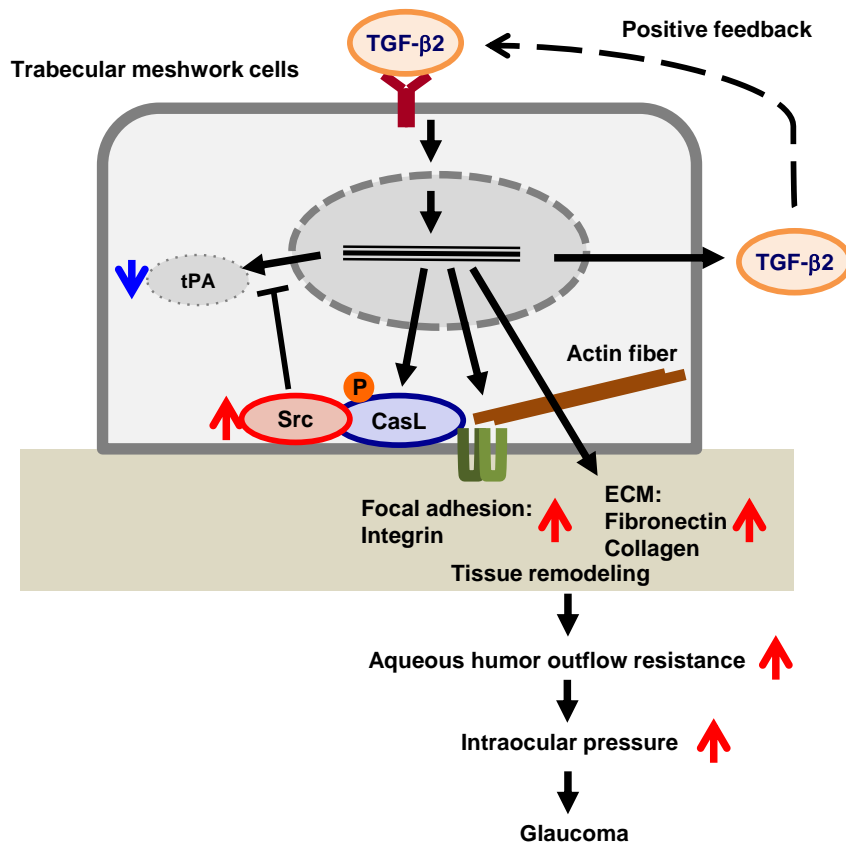


**Figure 25. Hypothetical mechanism for TGF- $\beta$ 2-induced IOP elevation in glaucoma.** TGF- $\beta$ 2 induces phosphorylation of Src and the upregulation of CasL, actin fiber, integrin, and ECM, resulting in formation of a focal adhesion complex. TGF- $\beta$ 2 is also upregulated through positive feedback. Upregulated CasL activates Src, which in turn downregulates tPA, which is involved in ECM degradation. These changes affect tissue remodeling, resulting in elevation of IOP by increasing resistance to aqueous humor outflow in the trabecular meshwork.

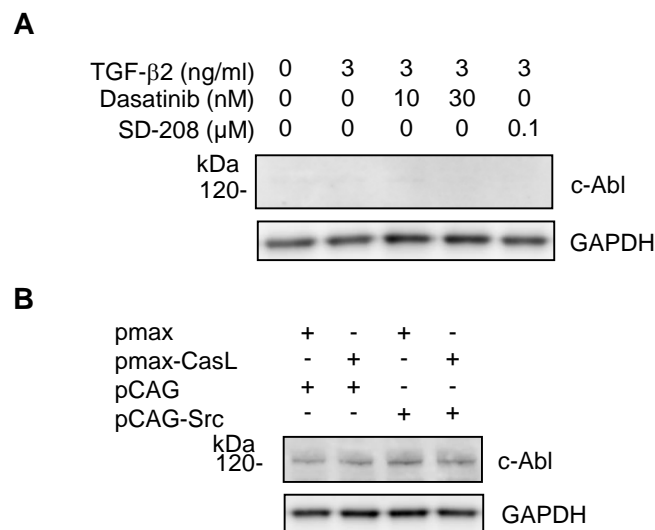


**Figure 26. Expression of c-Abl in trabecular meshwork cells and HepG2 cells.** (A) Trabecular meshwork cells were incubated with serum-free DMEM containing the indicated reagents for 48 h. Lysates were subjected to immunoblotting with the indicated antibodies. (B) HepG2 cells were transfected for 24 h with the indicated constructs in DMEM supplemented with 10% FBS. After incubation with serum-free DMEM for 24 h, total cell lysates were prepared and immunoblotted with the indicated antibodies.

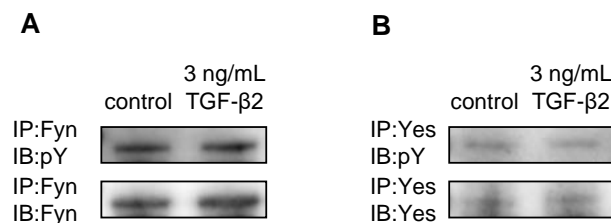


**Figure 27. Effects of TGF- $\beta$ 2 on the phosphorylation of Fyn and Yes.** (A) Anti-Fyn and (B) Anti-Yes immunoprecipitates from cells treated with or without 3 ng/mL TGF- $\beta$ 2 for 48 h in serum-free DMEM were subjected to immunoblotting with the indicated antibodies.

## Tables

**Table 1. Primer sequences for qRT-PCR**

Name	Sequence	
	Forward	Reverse
GAPDH	GCAGGGGGAGCCAAAAGGGT	TGGGTGGCAGTGTGGCATGG
tPA	TGTGCTGGAGACACTCGG	ACGAATCCAGTCTAGGTAGTTGG
CasL	GATGACTACGATTACGTCCACCTAC	CTCTGAGAGGGCTTCCACTTC
fibronectin1	CTGAACGTACATGCTTCGGT	AGATGGCTGTGGTGCATT
COL4A1	AGGCACAGGACCTTGGGA	GGGAGCCATCTCTTCCACTT
Integrin $\beta$ 3	TGCCCCAGAATCCATCGAGT	GGTTACTGGTGAGCTTCGCA
TGF- $\beta$ 2	CAAGAGCAGAAGGCGAATGG	TCACCACTGGTATATGTGGAGG
Myocilin	AGCAAGGCTGAGAAGGGG	GGCTCTCCTTCAAAATTGGGG

**Table 2. Representative ECM-related genes regulated by TGF- $\beta$ 2**

Protein name of down-regulated gene	Fold change	
	24 h	48 h
Plasminogen activator, tissue	0.39	0.82
ADAM metallopeptidase with thrombospondin type 1 motif, 9	0.07	0.16
ADAM metallopeptidase with thrombospondin type 1 motif, 14	0.26	0.16
ADAM metallopeptidase with thrombospondin type 1 motif, 19	0.62	0.49

Protein name of up-regulated gene	Fold change	
	24 h	48 h
Fibronectin 1	1.74	2.34
Elastin	5.02	4.27
Laminin, gamma 1	2.03	1.56
Laminin, gamma 2	6.82	10.27
Laminin, gamma 3	2.08	1.08
Collagen, type I, alpha 1	5.10	4.41
Collagen, type IV, alpha 2	4.00	3.54
Collagen, type VIII, alpha 2	13.09	13.45
Integrin, alpha V	2.53	2.16
Integrin, alpha 1	1.39	0.97
Integrin, beta 3	2.11	2.99
Transforming growth factor, beta 1	2.38	2.11
Transforming growth factor, beta 2	2.23	1.67

Data are presented as averages.

**Table 3. List of representative proteins identified by LC-MS/MS analysis**

<b>Identified proteins</b>	<b>Molecular</b>		<b>Probability</b>		
	<b>weight</b>	<b>sample1</b>	<b>sample2</b>	<b>sample3</b>	<b>sample4</b>
	<b>(kDa)</b>				
Focal adhesion kinase 1	119	64.61	51.31	82.37	54.6
Enhancer of filamentation 1 (CasL, NEDD9)	93	28.19	25.96	50.43	37.89
Programmed cell death 6-interacting protein	96	27.02	22.94	33.62	36.77
Breast cancer anti-estrogen resistance protein	93	14.1	19.92	18.49	24.52
Bone morphogenetic protein receptor type-2	115	9.4	13.88	15.13	15.6
Phosphatidylinositol 4,5-bisphosphate 3-kinase catalytic subunit alpha isoform	124	5.87	16.3	1.68	7.8
Ephrin type-B receptor 4	108	15.27	13.28	10.09	12.26
ATP-citrate synthase	121	14.1	13.28	8.4	11.14
Ras GTPase-activating protein 1	116	10.57	10.87	13.45	14.49
NEDD4-like E3 ubiquitin-protein ligase WWP2	99	10.57	11.47	11.77	11.14

**Table 4. List of ECM-related genes regulated by TGF- $\beta$ 2**

ProbeID	PrimaryAccession	GeneSymbol	3ng/mL TGF- $\beta$ 2		
			24h	48h	Description
A_33_P3212860	NM_212557	AMTN	34.30	12.73	Homo sapiens amelotin (AMTN), transcript variant 1, mRNA [NM_212557]
A_23_P6771	NM_014583	LMCD1	27.10	15.67	Homo sapiens LIM and cysteine-rich domains 1 (LMCD1), transcript variant 1, mRNA [NM_014583]
A_23_P7727	NM_001884	HAPLN1	18.77	28.25	Homo sapiens hyaluronan and proteoglycan link protein 1 (HAPLN1), mRNA [NM_001884]
A_23_P148990	NM_031935	HMCN1	17.15	21.71	Homo sapiens hemicentin 1 (HMCN1), mRNA [NM_031935]
A_24_P158089	NM_000602	SERPINE1	13.36	14.72	Homo sapiens serpin peptidase inhibitor, clade E (nexin, plasminogen activator inhibitor type 1), member 1 (SERPINE1), mRNA [NM_000602]
A_24_P365975	NM_005202	COL8A2	13.09	13.45	Homo sapiens collagen, type VIII, alpha 2 (COL8A2), transcript variant 1, mRNA [NM_005202]
A_33_P3511265	NM_006475	POSTN	12.47	16.11	Homo sapiens periostin, osteoblast specific factor (POSTN), transcript variant 1, mRNA [NM_006475]
A_23_P19663	NM_001901	CTGF	10.78	6.28	Homo sapiens connective tissue growth factor (CTGF), mRNA [NM_001901]
A_24_P264943	NM_000095	COMP	10.06	5.21	Homo sapiens cartilage oligomeric matrix protein (COMP), mRNA [NM_000095]
A_24_P185854	NM_004010	DMD	9.99	7.62	Homo sapiens dystrophin (DMD), transcript variant Dp427p2, mRNA [NM_004010]
A_23_P65240	NM_001845	COL4A1	9.92	7.16	Homo sapiens collagen, type IV, alpha 1 (COL4A1), transcript variant 1, mRNA [NM_001845]
A_23_P201636	NM_005562	LAMC2	6.82	10.27	Homo sapiens laminin, gamma 2 (LAMC2), transcript variant 1, mRNA [NM_005562]
A_23_P160968	NM_018891	LAMC2	6.54	11.39	Homo sapiens laminin, gamma 2 (LAMC2), transcript variant 2, mRNA [NM_018891]
A_23_P405129	NM_000428	LTBP2	6.36	7.26	Homo sapiens latent transforming growth factor beta binding protein 2 (LTBP2), mRNA [NM_000428]
A_23_P157865	NM_002160	TNC	5.86	9.78	Homo sapiens tenascin C (TNC), mRNA [NM_002160]
A_23_P7313	NM_001040058	SPP1	5.82	7.41	Homo sapiens secreted phosphoprotein 1 (SPP1), transcript variant 1, mRNA [NM_001040058]
A_23_P7313	NM_001040058	SPP1	5.78	11.39	Homo sapiens secreted phosphoprotein 1 (SPP1), transcript variant 1, mRNA [NM_001040058]
A_23_P151895	NM_003613	CILP	5.46	1.52	Homo sapiens cartilage intermediate layer protein, nucleotide pyrophosphohydrolase (CILP), mRNA [NM_003613]
A_23_P144071	NM_000094	COL7A1	5.35	6.15	Homo sapiens collagen, type VII, alpha 1 (COL7A1), mRNA [NM_000094]
A_23_P156327	NM_000358	TGFBI	5.24	2.68	Homo sapiens transforming growth factor, beta-induced, 68kDa (TGFBI), mRNA [NM_000358]
A_33_P3284763	NM_004021	DMD	5.21	5.62	Homo sapiens dystrophin (DMD), transcript variant Dp140b, mRNA [NM_004021]
A_33_P3304668	NM_000088	COL1A1	5.10	4.41	Homo sapiens collagen, type I, alpha 1 (COL1A1), mRNA [NM_000088]
A_33_P3629678	NM_000093	COL5A1	5.06	3.66	Homo sapiens collagen, type V, alpha 1 (COL5A1), transcript variant 1, mRNA [NM_000093]
A_23_P215454	NM_001278939	ELN	5.03	4.26	Homo sapiens elastin (ELN), transcript variant 13, mRNA [NM_001278939]
A_23_P7313	NM_001040058	SPP1	4.89	11.47	Homo sapiens secreted phosphoprotein 1 (SPP1), transcript variant 1, mRNA [NM_001040058]
A_24_P251969	NM_000800	FGF1	4.72	3.41	Homo sapiens fibroblast growth factor 1 (acidic) (FGF1), transcript variant 1, mRNA [NM_000800]
A_23_P50919	NM_006216	SERPINE2	4.66	4.63	Homo sapiens serpin peptidase inhibitor, clade E (nexin, plasminogen activator inhibitor type 1), member 2 (SERPINE2), transcript variant 1, mRNA [NM_006216]
A_23_P206022	NM_001004439	ITGA11	4.50	10.78	Homo sapiens integrin, alpha 11 (ITGA11), mRNA [NM_001004439]
A_23_P7313	NM_001040058	SPP1	4.44	16.68	Homo sapiens secreted phosphoprotein 1 (SPP1), transcript variant 1, mRNA [NM_001040058]
A_23_P144959	NM_004385	VCAN	4.35	4.44	Homo sapiens versican (VCAN), transcript variant 1, mRNA [NM_004385]
A_33_P3361636	NM_001190839	MGP	4.23	0.70	Homo sapiens matrix Gla protein (MGP), transcript variant 1, mRNA [NM_001190839]
A_23_P113701	NM_002607	PDGFA	4.11	3.10	Homo sapiens platelet-derived growth factor alpha polypeptide (PDGFA), transcript variant 1, mRNA [NM_002607]

3ng/mL TGF- $\beta$ 2					
ProbeID	PrimaryAccession	GeneSymbol	24h	48h	Description
A_23_P7313	NM_001040058	SPP1	4.08	24.42	Homo sapiens secreted phosphoprotein 1 (SPP1), transcript variant 1, mRNA [NM_001040058]
A_23_P97677	NM_002379	MATN1	4.06	1.71	Homo sapiens matrilin 1, cartilage matrix protein (MATN1), mRNA [NM_002379]
A_23_P205031	NM_001846	COL4A2	4.00	3.53	Homo sapiens collagen, type IV, alpha 2 (COL4A2), mRNA [NM_001846]
A_23_P7313	NM_001040058	SPP1	3.86	5.03	Homo sapiens secreted phosphoprotein 1 (SPP1), transcript variant 1, mRNA [NM_001040058]
A_22_P00003481	ENST00000473959	CCDC80	3.84	18.13	coiled-coil domain containing 80 [Source:HGNC Symbol;Acc:HGNC:30649] [ENST00000473959]
A_23_P102058	NM_002381	MATN3	3.76	4.99	Homo sapiens matrilin 3 (MATN3), mRNA [NM_002381]
A_33_P3708413	NM_003480	MFAP5	3.71	7.01	Homo sapiens microfibrillar associated protein 5 (MFAP5), transcript variant 1, mRNA [NM_003480]
A_23_P151805	NM_006329	FBLN5	3.66	3.20	Homo sapiens fibulin 5 (FBLN5), mRNA [NM_006329]
A_23_P204286	NM_000900	MGP	3.66	0.69	Homo sapiens matrix Gla protein (MGP), transcript variant 2, mRNA [NM_000900]
A_33_P3295358	NM_139314	ANGPTL4	3.63	0.86	Homo sapiens angiopoietin-like 4 (ANGPTL4), transcript variant 1, mRNA [NM_139314]
A_23_P7313	NM_001040058	SPP1	3.61	6.92	Homo sapiens secreted phosphoprotein 1 (SPP1), transcript variant 1, mRNA [NM_001040058]
A_23_P216429	NM_017680	ASPN	3.58	2.77	Homo sapiens asporin (ASPN), transcript variant 1, mRNA [NM_017680]
A_33_P3420466	NM_002381	MATN3	3.48	5.66	Homo sapiens matrilin 3 (MATN3), mRNA [NM_002381]
A_24_P354689	NM_004598	SPOCK1	3.43	2.93	Homo sapiens sparc/osteonectin, cwcv and kazal-like domains proteoglycan (testican) 1 (SPOCK1), mRNA [NM_004598]
A_23_P429950	NM_000216	KAL1	3.34	8.28	Homo sapiens Kallmann syndrome 1 sequence (KAL1), mRNA [NM_000216]
A_23_P64617	NM_012193	FZD4	3.23	3.16	Homo sapiens frizzled class receptor 4 (FZD4), mRNA [NM_012193]
A_23_P20697	NM_014694	ADAMTSL2	3.23	1.23	Homo sapiens ADAMTS-like 2 (ADAMTSL2), transcript variant 1, mRNA [NM_014694]
A_23_P7313	NM_001040058	SPP1	3.20	9.38	Homo sapiens secreted phosphoprotein 1 (SPP1), transcript variant 1, mRNA [NM_001040058]
A_23_P7313	NM_001040058	SPP1	3.20	20.53	Homo sapiens secreted phosphoprotein 1 (SPP1), transcript variant 1, mRNA [NM_001040058]
A_33_P3350703	NM_019891	ERO1LB	3.16	1.74	Homo sapiens ERO1-like beta (S. cerevisiae) (ERO1LB), mRNA [NM_019891]
A_23_P1029	NM_017459	MFAP2	3.16	2.83	Homo sapiens microfibrillar-associated protein 2 (MFAP2), transcript variant 1, mRNA [NM_017459]
A_33_P3216059	NM_001193335	ASPN	3.14	2.55	Homo sapiens asporin (ASPN), transcript variant 2, mRNA [NM_001193335]
A_23_P7313	NM_001040058	SPP1	3.14	7.62	Homo sapiens secreted phosphoprotein 1 (SPP1), transcript variant 1, mRNA [NM_001040058]
A_23_P10206	NM_005328	HAS2	3.10	1.53	Homo sapiens hyaluronan synthase 2 (HAS2), mRNA [NM_005328]
A_23_P164057	NM_002404	MFAP4	2.97	3.36	Homo sapiens microfibrillar-associated protein 4 (MFAP4), transcript variant 2, mRNA [NM_002404]
A_33_P3237135	NM_004530	MMP2	2.91	3.14	Homo sapiens matrix metalloproteinase 2 (gelatinase A, 72kDa gelatinase, 72kDa type IV collagenase) (MMP2), transcript variant 1, mRNA [NM_004530]
A_23_P46429	NM_001554	CYR61	2.91	3.01	Homo sapiens cysteine-rich, angiogenic inducer, 61 (CYR61), mRNA [NM_001554]
A_23_P83818	NM_000093	COL5A1	2.89	2.73	Homo sapiens collagen, type V, alpha 1 (COL5A1), transcript variant 1, mRNA [NM_000093]
A_23_P34126	NM_001711	BGN	2.87	3.58	Homo sapiens biglycan (BGN), mRNA [NM_001711]
A_24_P62505	NM_015101	COLGALT2	2.87	2.97	Homo sapiens collagen beta(1-O)galactosyltransferase 2 (COLGALT2), transcript variant 1, mRNA [NM_015101]
A_23_P353035	NM_001553	IGFBP7	2.77	4.20	Homo sapiens insulin-like growth factor binding protein 7 (IGFBP7), transcript variant 1, mRNA [NM_001553]

3ng/mL TGF- $\beta$ 2					
ProbeID	PrimaryAccession	GeneSymbol	24h	48h	Description
A_33_P3251896	NM_004307	APBB2	2.75	2.69	Homo sapiens amyloid beta (A4) precursor protein-binding, family B, member 2 (APBB2), transcript variant 1, mRNA [NM_004307]
A_23_P360754	NM_005099	ADAMTS4	2.71	1.59	Homo sapiens ADAM metallopeptidase with thrombospondin type 1 motif, 4 (ADAMTS4), mRNA [NM_005099]
A_33_P3419696	NM_002006	FGF2	2.71	2.00	Homo sapiens fibroblast growth factor 2 (basic) (FGF2), mRNA [NM_002006]
A_23_P82990	NM_033014	OGN	2.69	0.48	Homo sapiens osteoglycin (OGN), transcript variant 1, mRNA [NM_033014]
A_22_P00025671	ENST00000295666	IGFBP7	2.68	4.82	insulin-like growth factor binding protein 7 [Source:HGNC Symbol;Acc:HGNC:5476] [ENST00000295666]
A_33_P3313283	NM_153221	CILP2	2.68	2.95	Homo sapiens cartilage intermediate layer protein 2 (CILP2), mRNA [NM_153221]
A_33_P3416218	NM_005960	MUC3A	2.64	1.26	Homo sapiens mucin 3A, cell surface associated (MUC3A), mRNA [NM_005960]
A_23_P213336	NM_000800	FGF1	2.57	3.56	Homo sapiens fibroblast growth factor 1 (acidic) (FGF1), transcript variant 1, mRNA [NM_000800]
A_23_P106602	NM_031476	CRISPLD2	2.55	1.00	Homo sapiens cysteine-rich secretory protein LCCL domain containing 2 (CRISPLD2), mRNA [NM_031476]
A_22_P00017060	NM_001164489	ADAM8	2.55	3.53	Homo sapiens ADAM metallopeptidase domain 8 (ADAM8), transcript variant 2, mRNA [NM_001164489]
A_23_P26847	NM_000346	SOX9	2.55	5.50	Homo sapiens SRY (sex determining region Y)-box 9 (SOX9), mRNA [NM_000346]
A_23_P50907	NM_002210	ITGAV	2.53	2.16	Homo sapiens integrin, alpha V (ITGAV), transcript variant 1, mRNA [NM_002210]
A_23_P50907	NM_002210	ITGAV	2.45	2.16	Homo sapiens integrin, alpha V (ITGAV), transcript variant 1, mRNA [NM_002210]
A_22_P00008038	NM_001253835	IGFBP7	2.43	3.84	Homo sapiens insulin-like growth factor binding protein 7 (IGFBP7), transcript variant 2, mRNA [NM_001253835]
A_23_P50907	NM_002210	ITGAV	2.43	2.22	Homo sapiens integrin, alpha V (ITGAV), transcript variant 1, mRNA [NM_002210]
A_33_P3321070	ENST00000415567	WNT4	2.41	2.31	wingless-type MMTV integration site family, member 4 [Source:HGNC Symbol;Acc:HGNC:12783] [ENST00000415567]
A_33_P3379886	NM_002006	FGF2	2.41	1.88	Homo sapiens fibroblast growth factor 2 (basic) (FGF2), mRNA [NM_002006]
A_23_P50907	NM_002210	ITGAV	2.41	2.19	Homo sapiens integrin, alpha V (ITGAV), transcript variant 1, mRNA [NM_002210]
A_23_P50907	NM_002210	ITGAV	2.39	2.22	Homo sapiens integrin, alpha V (ITGAV), transcript variant 1, mRNA [NM_002210]
A_33_P3326643	NM_001277269	OTOG	2.38	1.73	Homo sapiens otogelin (OTOG), transcript variant 1, mRNA [NM_001277269]
A_23_P50907	NM_002210	ITGAV	2.38	2.22	Homo sapiens integrin, alpha V (ITGAV), transcript variant 1, mRNA [NM_002210]
A_23_P50907	NM_002210	ITGAV	2.38	2.16	Homo sapiens integrin, alpha V (ITGAV), transcript variant 1, mRNA [NM_002210]
A_23_P122216	NM_002317	LOX	2.38	2.69	Homo sapiens lysyl oxidase (LOX), transcript variant 1, mRNA [NM_002317]
A_24_P79054	NM_000660	TGFB1	2.38	2.10	Homo sapiens transforming growth factor, beta 1 (TGFB1), mRNA [NM_000660]
A_23_P122216	NM_002317	LOX	2.36	2.69	Homo sapiens lysyl oxidase (LOX), transcript variant 1, mRNA [NM_002317]
A_23_P50907	NM_002210	ITGAV	2.36	2.17	Homo sapiens integrin, alpha V (ITGAV), transcript variant 1, mRNA [NM_002210]
A_23_P122216	NM_002317	LOX	2.36	2.69	Homo sapiens lysyl oxidase (LOX), transcript variant 1, mRNA [NM_002317]
A_23_P122216	NM_002317	LOX	2.36	2.66	Homo sapiens lysyl oxidase (LOX), transcript variant 1, mRNA [NM_002317]
A_23_P122216	NM_002317	LOX	2.36	2.75	Homo sapiens lysyl oxidase (LOX), transcript variant 1, mRNA [NM_002317]
A_23_P122216	NM_002317	LOX	2.35	2.66	Homo sapiens lysyl oxidase (LOX), transcript variant 1, mRNA [NM_002317]
A_23_P122216	NM_002317	LOX	2.35	2.69	Homo sapiens lysyl oxidase (LOX), transcript variant 1, mRNA [NM_002317]

3ng/mL TGF- $\beta$ 2					
ProbeID	PrimaryAccession	GeneSymbol	24h	48h	Description
A_23_P122216	NM_002317	LOX	2.35	2.73	Homo sapiens lysyl oxidase (LOX), transcript variant 1, mRNA [NM_002317]
A_23_P50907	NM_002210	ITGAV	2.33	2.20	Homo sapiens integrin, alpha V (ITGAV), transcript variant 1, mRNA [NM_002210]
A_23_P50907	NM_002210	ITGAV	2.31	2.16	Homo sapiens integrin, alpha V (ITGAV), transcript variant 1, mRNA [NM_002210]
A_23_P122216	NM_002317	LOX	2.31	2.66	Homo sapiens lysyl oxidase (LOX), transcript variant 1, mRNA [NM_002317]
A_23_P122216	NM_002317	LOX	2.31	2.64	Homo sapiens lysyl oxidase (LOX), transcript variant 1, mRNA [NM_002317]
A_24_P402438	NM_003238	TGFB2	2.23	1.67	Homo sapiens transforming growth factor, beta 2 (TGFB2), transcript variant 2, mRNA [NM_003238]
A_24_P71973	NM_002253	KDR	2.22	1.67	Homo sapiens kinase insert domain receptor (a type III receptor tyrosine kinase) (KDR), mRNA [NM_002253]
A_33_P3348239	NM_000138	FBN1	2.22	2.38	Homo sapiens fibrillin 1 (FBN1), mRNA [NM_000138]
A_24_P184799	NM_004086	COCH	2.20	5.82	Homo sapiens cochli (COCH), transcript variant 2, mRNA [NM_004086]
A_23_P105957	NM_001102	ACTN1	2.17	1.77	Homo sapiens actinin, alpha 1 (ACTN1), transcript variant 2, mRNA [NM_001102]
A_22_P000019155	ENST00000473959	CCDC80	2.14	3.56	coiled-coil domain containing 80 [Source:HGNC Symbol;Acc:HGNC:30649] [ENST00000473959]
A_33_P3382924	NM_003118	SPARC	2.14	1.96	Homo sapiens secreted protein, acidic, cysteine-rich (osteonectin) (SPARC), mRNA [NM_003118]
A_24_P318656	NM_000212	ITGB3	2.11	2.99	Homo sapiens integrin, beta 3 (platelet glycoprotein IIIa, antigen CD61) (ITGB3), mRNA [NM_000212]
A_23_P82979	NM_006059	LAMC3	2.08	1.08	Homo sapiens laminin, gamma 3 (LAMC3), mRNA [NM_006059]
A_33_P3216568	XM_006709945	MUC5AC	2.07	2.25	PREDICTED: Homo sapiens mucin 5AC, oligomeric mucus/gel-forming (MUC5AC), partial mRNA [XM_006709945]
A_23_P74701	NM_152890	COL24A1	2.06	1.95	Homo sapiens collagen, type XXIV, alpha 1 (COL24A1), mRNA [NM_152890]
A_23_P160318	NM_001856	COL16A1	2.04	2.33	Homo sapiens collagen, type XVI, alpha 1 (COL16A1), mRNA [NM_001856]
A_24_P270033	NM_198275	MPZL3	2.03	2.89	Homo sapiens myelin protein zero-like 3 (MPZL3), transcript variant 1, mRNA [NM_198275]
A_33_P3237150	NM_001200	BMP2	2.03	1.40	Homo sapiens bone morphogenetic protein 2 (BMP2), mRNA [NM_001200]
A_23_P201628	NM_002293	LAMC1	2.03	1.56	Homo sapiens laminin, gamma 1 (formerly LAMB2) (LAMC1), mRNA [NM_002293]
A_33_P3238166	NM_012293	PXDN	2.01	2.07	Homo sapiens peroxidasin (PXDN), mRNA [NM_012293]
A_23_P435407	NM_001448	GPC4	2.01	1.29	Homo sapiens glypican 4 (GPC4), mRNA [NM_001448]
A_33_P3216570	XM_006709945	MUC5AC	2.01	1.20	PREDICTED: Homo sapiens mucin 5AC, oligomeric mucus/gel-forming (MUC5AC), partial mRNA [XM_006709945]
A_23_P111888	NM_138455	CTHRC1	1.99	2.10	Homo sapiens collagen triple helix repeat containing 1 (CTHRC1), transcript variant 1, mRNA [NM_138455]
A_33_P3271455	NM_012293	PXDN	1.95	2.01	Homo sapiens peroxidasin (PXDN), mRNA [NM_012293]
A_23_P303671	NM_001393	ECM2	1.93	1.74	Homo sapiens extracellular matrix protein 2, female organ and adipocyte specific (ECM2), transcript variant 1, mRNA [NM_001393]
A_21_P0000156	NM_001204760	TLL1	1.93	1.31	Homo sapiens tollloid-like 1 (TLL1), transcript variant 2, mRNA [NM_001204760]
A_33_P3221284	NM_199511	CCDC80	1.89	1.44	Homo sapiens coiled-coil domain containing 80 (CCDC80), transcript variant 1, mRNA [NM_199511]
A_33_P3210488	NM_004369	COL6A3	1.79	2.22	Homo sapiens collagen, type VI, alpha 3 (COL6A3), transcript variant 1, mRNA [NM_004369]
A_24_P334130	NM_054034	FN1	1.74	2.35	Homo sapiens fibronectin 1 (FN1), transcript variant 7, mRNA [NM_054034]
A_23_P214144	NM_000493	COL10A1	1.72	2.62	Homo sapiens collagen, type X, alpha 1 (COL10A1), mRNA [NM_000493]

3ng/mL TGF- $\beta$ 2					
ProbeID	PrimaryAccession	GeneSymbol	24h	48h	Description
A_23_P122216	NM_002317	LOX	2.35	2.73	Homo sapiens lysyl oxidase (LOX), transcript variant 1, mRNA [NM_002317]
A_23_P50907	NM_002210	ITGAV	2.33	2.20	Homo sapiens integrin, alpha V (ITGAV), transcript variant 1, mRNA [NM_002210]
A_23_P50907	NM_002210	ITGAV	2.31	2.16	Homo sapiens integrin, alpha V (ITGAV), transcript variant 1, mRNA [NM_002210]
A_23_P122216	NM_002317	LOX	2.31	2.66	Homo sapiens lysyl oxidase (LOX), transcript variant 1, mRNA [NM_002317]
A_23_P122216	NM_002317	LOX	2.31	2.64	Homo sapiens lysyl oxidase (LOX), transcript variant 1, mRNA [NM_002317]
A_24_P402438	NM_003238	TGFB2	2.23	1.67	Homo sapiens transforming growth factor, beta 2 (TGFB2), transcript variant 2, mRNA [NM_003238]
A_24_P71973	NM_002253	KDR	2.22	1.67	Homo sapiens kinase insert domain receptor (a type III receptor tyrosine kinase) (KDR), mRNA [NM_002253]
A_33_P3348239	NM_000138	FBN1	2.22	2.38	Homo sapiens fibrillin 1 (FBN1), mRNA [NM_000138]
A_24_P184799	NM_004086	COCH	2.20	5.82	Homo sapiens cochli (COCH), transcript variant 2, mRNA [NM_004086]
A_23_P105957	NM_001102	ACTN1	2.17	1.77	Homo sapiens actinin, alpha 1 (ACTN1), transcript variant 2, mRNA [NM_001102]
A_22_P000019155	ENST00000473959	CCDC80	2.14	3.56	coiled-coil domain containing 80 [Source:HGNC Symbol;Acc:HGNC:30649] [ENST00000473959]
A_33_P3382924	NM_003118	SPARC	2.14	1.96	Homo sapiens secreted protein, acidic, cysteine-rich (osteonectin) (SPARC), mRNA [NM_003118]
A_24_P318656	NM_000212	ITGB3	2.11	2.99	Homo sapiens integrin, beta 3 (platelet glycoprotein IIIa, antigen CD61) (ITGB3), mRNA [NM_000212]
A_23_P82979	NM_006059	LAMC3	2.08	1.08	Homo sapiens laminin, gamma 3 (LAMC3), mRNA [NM_006059]
A_33_P3216568	XM_006709945	MUC5AC	2.07	2.25	PREDICTED: Homo sapiens mucin 5AC, oligomeric mucus/gel-forming (MUC5AC), partial mRNA [XM_006709945]
A_23_P74701	NM_152890	COL24A1	2.06	1.95	Homo sapiens collagen, type XXIV, alpha 1 (COL24A1), mRNA [NM_152890]
A_23_P160318	NM_001856	COL16A1	2.04	2.33	Homo sapiens collagen, type XVI, alpha 1 (COL16A1), mRNA [NM_001856]
A_24_P270033	NM_198275	MPZL3	2.03	2.89	Homo sapiens myelin protein zero-like 3 (MPZL3), transcript variant 1, mRNA [NM_198275]
A_33_P3237150	NM_001200	BMP2	2.03	1.40	Homo sapiens bone morphogenetic protein 2 (BMP2), mRNA [NM_001200]
A_23_P201628	NM_002293	LAMC1	2.03	1.56	Homo sapiens laminin, gamma 1 (formerly LAMB2) (LAMC1), mRNA [NM_002293]
A_33_P3238166	NM_012293	PXDN	2.01	2.07	Homo sapiens peroxidasin (PXDN), mRNA [NM_012293]
A_23_P435407	NM_001448	GPC4	2.01	1.29	Homo sapiens glypican 4 (GPC4), mRNA [NM_001448]
A_33_P3216570	XM_006709945	MUC5AC	2.01	1.20	PREDICTED: Homo sapiens mucin 5AC, oligomeric mucus/gel-forming (MUC5AC), partial mRNA [XM_006709945]
A_23_P111888	NM_138455	CTHRC1	1.99	2.10	Homo sapiens collagen triple helix repeat containing 1 (CTHRC1), transcript variant 1, mRNA [NM_138455]
A_33_P3271455	NM_012293	PXDN	1.95	2.01	Homo sapiens peroxidasin (PXDN), mRNA [NM_012293]
A_23_P303671	NM_001393	ECM2	1.93	1.74	Homo sapiens extracellular matrix protein 2, female organ and adipocyte specific (ECM2), transcript variant 1, mRNA [NM_001393]
A_21_P0000156	NM_001204760	TLL1	1.93	1.31	Homo sapiens tollloid-like 1 (TLL1), transcript variant 2, mRNA [NM_001204760]
A_33_P3221284	NM_199511	CCDC80	1.89	1.44	Homo sapiens coiled-coil domain containing 80 (CCDC80), transcript variant 1, mRNA [NM_199511]
A_33_P3210488	NM_004369	COL6A3	1.79	2.22	Homo sapiens collagen, type VI, alpha 3 (COL6A3), transcript variant 1, mRNA [NM_004369]
A_24_P334130	NM_054034	FN1	1.74	2.35	Homo sapiens fibronectin 1 (FN1), transcript variant 7, mRNA [NM_054034]
A_23_P214144	NM_000493	COL10A1	1.72	2.62	Homo sapiens collagen, type X, alpha 1 (COL10A1), mRNA [NM_000493]

3ng/mL TGF- $\beta$ 2					
ProbeID	PrimaryAccession	GeneSymbol	24h	48h	Description
A_23_P55251	NM_002204	ITGA3	1.66	2.03	Homo sapiens integrin, alpha 3 (antigen CD49C, alpha 3 subunit of VLA-3 receptor) (ITGA3), transcript variant a, mRNA [NM_002204]
A_23_P213319	NM_197941	ADAMTS6	1.65	2.03	Homo sapiens ADAM metallopeptidase with thrombospondin type 1 motif, 6 (ADAMTS6), mRNA [NM_197941]
A_23_P34345	NM_001078	VCAM1	1.65	3.39	Homo sapiens vascular cell adhesion molecule 1 (VCAM1), transcript variant 1, mRNA [NM_001078]
A_24_P12401	NM_001025366	VEGFA	1.57	2.36	Homo sapiens vascular endothelial growth factor A (VEGFA), transcript variant 1, mRNA [NM_001025366]
A_33_P3259339	NM_080629	COL11A1	1.54	2.10	Homo sapiens collagen, type XI, alpha 1 (COL11A1), transcript variant B, mRNA [NM_080629]
A_23_P97096	NM_014359	OPTC	1.54	4.76	Homo sapiens optin (OPTC), mRNA [NM_014359]
A_33_P3383351	ENST00000464187	COL5A1	1.45	2.01	collagen, type V, alpha 1 [Source:HGNC Symbol;Acc:HGNC:2209] [ENST00000464187]
A_23_P118571	NM_025237	SOST	1.45	5.24	Homo sapiens sclerostin (SOST), mRNA [NM_025237]
A_33_P3297930	NM_005202	COL8A2	1.44	1.92	Homo sapiens collagen, type VIII, alpha 2 (COL8A2), transcript variant 1, mRNA [NM_005202]
A_24_P189997	NM_138322	PCSK6	1.43	2.77	Homo sapiens proprotein convertase subtilisin/kexin type 6 (PCSK6), transcript variant 3, mRNA [NM_138322]
A_33_P3353791	NM_181501	ITGA1	1.39	0.97	Homo sapiens integrin, alpha 1 (ITGA1), mRNA [NM_181501]
A_33_P3405213	NM_000442	PECAM1	1.38	2.04	Homo sapiens platelet/endothelial cell adhesion molecule 1 (PECAM1), mRNA [NM_000442]
A_33_P3227400	NM_000092	COL4A4	1.34	2.99	Homo sapiens collagen, type IV, alpha 4 (COL4A4), mRNA [NM_000092]
A_23_P115261	NM_000029	AGT	1.26	0.27	Homo sapiens angiotensinogen (serpin peptidase inhibitor, clade A, member 8) (AGT), mRNA [NM_000029]
A_33_P3326634	NM_001164617	GPC3	1.23	0.27	Homo sapiens glypican 3 (GPC3), transcript variant 1, mRNA [NM_001164617]
A_23_P411157	NM_005430	WNT1	1.22	3.03	Homo sapiens wingless-type MMTV integration site family, member 1 (WNT1), mRNA [NM_005430]
A_33_P3272568	ENST00000379331	PRDX4	1.21	1.04	peroxiredoxin 4 [Source:HGNC Symbol;Acc:HGNC:17169] [ENST00000379331]
A_23_P44648	NM_030955	ADAMTS12	1.20	1.52	Homo sapiens ADAM metallopeptidase with thrombospondin type 1 motif, 12 (ADAMTS12), mRNA [NM_030955]
A_23_P115261	NM_000029	AGT	1.18	0.25	Homo sapiens angiotensinogen (serpin peptidase inhibitor, clade A, member 8) (AGT), mRNA [NM_000029]
A_23_P214026	NM_001999	FBN2	1.12	1.01	Homo sapiens fibrillin 2 (FBN2), mRNA [NM_001999]
A_33_P3243028	NM_014208	DSPP	1.11	2.38	Homo sapiens dentin sialophosphoprotein (DSPP), mRNA [NM_014208]
A_33_P3241051	NM_139057	ADAMTS17	1.11	2.55	Homo sapiens ADAM metallopeptidase with thrombospondin type 1 motif, 17 (ADAMTS17), mRNA [NM_139057]
A_23_P146456	NM_001333	CTSV	1.11	0.91	Homo sapiens cathepsin V (CTSV), transcript variant 1, mRNA [NM_001333]
A_24_P65373	NM_000419	ITGA2B	1.09	0.41	Homo sapiens integrin, alpha 2b (platelet glycoprotein IIb of IIb/IIIa complex, antigen CD41) (ITGA2B), mRNA [NM_000419]
A_33_P3281191	NM_002508	NID1	1.09	1.26	Homo sapiens nidogen 1 (NID1), mRNA [NM_002508]
A_23_P115261	NM_000029	AGT	1.07	0.30	Homo sapiens angiotensinogen (serpin peptidase inhibitor, clade A, member 8) (AGT), mRNA [NM_000029]
A_23_P115261	NM_000029	AGT	1.06	0.26	Homo sapiens angiotensinogen (serpin peptidase inhibitor, clade A, member 8) (AGT), mRNA [NM_000029]
A_23_P116898	NM_000014	A2M	1.05	0.12	Homo sapiens alpha-2-macroglobulin (A2M), mRNA [NM_000014]
A_23_P116898	NM_000014	A2M	1.03	0.15	Homo sapiens alpha-2-macroglobulin (A2M), mRNA [NM_000014]
A_24_P253003	NM_004626	WNT11	1.01	0.41	Homo sapiens wingless-type MMTV integration site family, member 11 (WNT11), mRNA [NM_004626]
A_23_P253896	NM_001033047	NPNT	1.00	0.64	Homo sapiens nephronectin (NPNT), transcript variant 2, mRNA [NM_001033047]

3ng/mL TGF- $\beta$ 2					
ProbeID	PrimaryAccession	GeneSymbol	24h	48h	Description
A_33_P3273669	NM_004801	NRXN1	1.00	2.36	Homo sapiens neurexin 1 (NRXN1), transcript variant alpha1, mRNA [NM_004801]
A_23_P116898	NM_000014	A2M	1.00	0.14	Homo sapiens alpha-2-macroglobulin (A2M), mRNA [NM_000014]
A_23_P149189	NM_021186	ZP4	1.00	0.16	Homo sapiens zona pellucida glycoprotein 4 (ZP4), mRNA [NM_021186]
A_23_P70307	NM_022138	SMOC2	1.00	0.43	Homo sapiens SPARC related modular calcium binding 2 (SMOC2), transcript variant 1, mRNA [NM_022138]
A_32_P133072	NM_006108	SPON1	1.00	1.00	Homo sapiens spondin 1, extracellular matrix protein (SPON1), mRNA [NM_006108]
A_23_P94397	NM_005014	OMD	1.00	1.00	Homo sapiens osteomodulin (OMD), mRNA [NM_005014]
A_23_P115261	NM_000029	AGT	0.98	0.24	Homo sapiens angiotensinogen (serpin peptidase inhibitor, clade A, member 8) (AGT), mRNA [NM_000029]
A_33_P3353816	NM_000885	ITGA4	0.97	0.91	Homo sapiens integrin, alpha 4 (antigen CD49D, alpha 4 subunit of VLA-4 receptor) (ITGA4), mRNA [NM_000885]
A_23_P154643	NM_001719	BMP7	0.96	1.21	Homo sapiens bone morphogenetic protein 7 (BMP7), mRNA [NM_001719]
A_23_P26976	NM_001267	CHAD	0.94	2.13	Homo sapiens chondroadherin (CHAD), mRNA [NM_001267]
A_23_P393034	NM_005329	HAS3	0.93	1.75	Homo sapiens hyaluronan synthase 3 (HAS3), transcript variant 1, mRNA [NM_005329]
A_23_P307310	NM_013227	ACAN	0.92	0.47	Homo sapiens aggrecan (ACAN), transcript variant 2, mRNA [NM_013227]
A_23_P115261	NM_000029	AGT	0.91	0.23	Homo sapiens angiotensinogen (serpin peptidase inhibitor, clade A, member 8) (AGT), mRNA [NM_000029]
A_23_P116898	NM_000014	A2M	0.90	0.11	Homo sapiens alpha-2-macroglobulin (A2M), mRNA [NM_000014]
A_33_P3234043	ENST00000471755	BMP1	0.90	3.56	bone morphogenetic protein 1 [Source:HGNC Symbol;Acc:HGNC:1067] [ENST00000471755]
A_23_P115261	NM_000029	AGT	0.90	0.31	Homo sapiens angiotensinogen (serpin peptidase inhibitor, clade A, member 8) (AGT), mRNA [NM_000029]
A_33_P3380642	AK027833	FRAS1	0.89	0.70	Homo sapiens cDNA FLJ14927 fis, clone PLACE1009094, weakly similar to FURIN-LIKE PROTEASE 2 PRECURSOR (EC 3.4.21.75). [AK027833]
A_23_P115261	NM_000029	AGT	0.89	0.24	Homo sapiens angiotensinogen (serpin peptidase inhibitor, clade A, member 8) (AGT), mRNA [NM_000029]
A_33_P3338121	NM_001017402	LAMB3	0.88	0.40	Homo sapiens laminin, beta 3 (LAMB3), transcript variant 2, mRNA [NM_001017402]
A_23_P1691	NM_002421	MMP1	0.86	1.00	Homo sapiens matrix metallopeptidase 1 (interstitial collagenase) (MMP1), transcript variant 1, mRNA [NM_002421]
A_24_P307135	NM_019105	TNXB	0.86	1.65	Homo sapiens tenascin XB (TNXB), transcript variant XB, mRNA [NM_019105]
A_23_P1691	NM_002421	MMP1	0.86	0.99	Homo sapiens matrix metallopeptidase 1 (interstitial collagenase) (MMP1), transcript variant 1, mRNA [NM_002421]
A_23_P1691	NM_002421	MMP1	0.86	1.02	Homo sapiens matrix metallopeptidase 1 (interstitial collagenase) (MMP1), transcript variant 1, mRNA [NM_002421]
A_23_P1691	NM_002421	MMP1	0.85	0.99	Homo sapiens matrix metallopeptidase 1 (interstitial collagenase) (MMP1), transcript variant 1, mRNA [NM_002421]
A_23_P1691	NM_002421	MMP1	0.85	0.99	Homo sapiens matrix metallopeptidase 1 (interstitial collagenase) (MMP1), transcript variant 1, mRNA [NM_002421]
A_23_P1691	NM_002421	MMP1	0.84	1.03	Homo sapiens matrix metallopeptidase 1 (interstitial collagenase) (MMP1), transcript variant 1, mRNA [NM_002421]
A_23_P1691	NM_002421	MMP1	0.84	1.00	Homo sapiens matrix metallopeptidase 1 (interstitial collagenase) (MMP1), transcript variant 1, mRNA [NM_002421]
A_23_P115261	NM_000029	AGT	0.84	0.27	Homo sapiens angiotensinogen (serpin peptidase inhibitor, clade A, member 8) (AGT), mRNA [NM_000029]
A_23_P40108	NM_001853	COL9A3	0.84	0.36	Homo sapiens collagen, type IX, alpha 3 (COL9A3), mRNA [NM_001853]
A_23_P1691	NM_002421	MMP1	0.84	0.99	Homo sapiens matrix metallopeptidase 1 (interstitial collagenase) (MMP1), transcript variant 1, mRNA [NM_002421]
A_23_P1691	NM_002421	MMP1	0.84	0.99	Homo sapiens matrix metallopeptidase 1 (interstitial collagenase) (MMP1), transcript variant 1, mRNA [NM_002421]

3ng/mL TGF- $\beta$ 2					
ProbeID	PrimaryAccession	GeneSymbol	24h	48h	Description
A_23_P1691	NM_002421	MMP1	0.84	1.00	Homo sapiens matrix metallopeptidase 1 (interstitial collagenase) (MMP1), transcript variant 1, mRNA [NM_002421]
A_23_P88404	NM_003239	TGFB3	0.81	0.46	Homo sapiens transforming growth factor, beta 3 (TGFB3), mRNA [NM_003239]
A_24_P353619	NM_000478	ALPL	0.81	0.70	Homo sapiens alkaline phosphatase, liver/bone/kidney (ALPL), transcript variant 1, mRNA [NM_000478]
A_32_P107876	NM_025074	FRAS1	0.79	0.63	Homo sapiens Fraser extracellular matrix complex subunit 1 (FRAS1), transcript variant 1, mRNA [NM_025074]
A_23_P158096	NM_032888	COL27A1	0.78	0.47	Homo sapiens collagen, type XXVII, alpha 1 (COL27A1), mRNA [NM_032888]
A_23_P115261	NM_000029	AGT	0.77	0.25	Homo sapiens angiotsinogen (serpin peptidase inhibitor, clade A, member 8) (AGT), mRNA [NM_000029]
A_23_P138524	NM_198148	CPXM2	0.76	0.70	Homo sapiens carboxypeptidase X (M14 family), member 2 (CPXM2), mRNA [NM_198148]
A_23_P83028	NM_021111	RECK	0.74	0.50	Homo sapiens reversion-inducing-cysteine-rich protein with kazal motifs (RECK), mRNA [NM_021111]
A_23_P207345	NM_002390	ADAM11	0.71	0.12	Homo sapiens ADAM metallopeptidase domain 11 (ADAM11), mRNA [NM_002390]
A_24_P759477	NM_002214	ITGB8	0.71	0.44	Homo sapiens integrin, beta 8 (ITGB8), mRNA [NM_002214]
A_33_P3413114	NM_052866	ADAMTSL1	0.69	0.50	Homo sapiens ADAMTS-like 1 (ADAMTSL1), transcript variant 2, mRNA [NM_052866]
A_33_P3302025	NM_052866	ADAMTSL1	0.66	0.49	Homo sapiens ADAMTS-like 1 (ADAMTSL1), transcript variant 2, mRNA [NM_052866]
A_33_P3363804	NM_001242608	NCAM1	0.65	0.45	Homo sapiens neural cell adhesion molecule 1 (NCAM1), transcript variant 4, mRNA [NM_001242608]
A_23_P114883	NM_002023	FMOD	0.64	0.23	Homo sapiens fibromodulin (FMOD), transcript variant 1, mRNA [NM_002023]
A_33_P3248903	NM_058238	WNT7B	0.63	1.09	Homo sapiens wingless-type MMTV integration site family, member 7B (WNT7B), mRNA [NM_058238]
A_33_P3317392	NM_133638	ADAMTS19	0.62	0.49	Homo sapiens ADAM metallopeptidase with thrombospondin type 1 motif, 19 (ADAMTS19), mRNA [NM_133638]
A_23_P251499	NM_002593	PCOLCE	0.61	0.48	Homo sapiens procollagen C-endopeptidase enhancer (PCOLCE), mRNA [NM_002593]
A_32_P32254	NM_001848	COL6A1	0.61	0.46	Homo sapiens collagen, type VI, alpha 1 (COL6A1), mRNA [NM_001848]
A_33_P3223592	NM_001302688	APOE	0.61	0.34	Homo sapiens apolipoprotein E (APOE), transcript variant 1, mRNA [NM_001302688]
A_23_P1331	NM_080801	COL13A1	0.60	0.99	Homo sapiens collagen, type XIII, alpha 1 (COL13A1), transcript variant 5, mRNA [NM_080801]
A_23_P59807	NM_003391	WNT2	0.59	0.38	Homo sapiens wingless-type MMTV integration site family member 2 (WNT2), transcript variant 1, mRNA [NM_003391]
A_23_P109034	NM_002999	SDC4	0.58	0.44	Homo sapiens syndecan 4 (SDC4), mRNA [NM_002999]
A_23_P433016	NM_001996	FBLN1	0.56	0.32	Homo sapiens fibulin 1 (FBLN1), transcript variant C, mRNA [NM_001996]
A_23_P215913	NM_001831	CLU	0.56	0.42	Homo sapiens clusterin (CLU), transcript variant 1, mRNA [NM_001831]
A_23_P128084	NM_002206	ITGA7	0.55	0.49	Homo sapiens integrin, alpha 7 (ITGA7), transcript variant 2, mRNA [NM_002206]
A_33_P3249872	NM_001996	FBLN1	0.54	0.31	Homo sapiens fibulin 1 (FBLN1), transcript variant C, mRNA [NM_001996]
A_23_P212042	NM_005929	MFI2	0.54	0.39	Homo sapiens antigen p97 (melanoma associated) identified by monoclonal antibodies 133.2 and 96.5 (MFI2), transcript variant 1, mRNA [NM_005929]
A_23_P109269	NM_005560	LAMA5	0.54	0.40	Homo sapiens laminin, alpha 5 (LAMA5), mRNA [NM_005560]
A_23_P57417	NM_005940	MMP11	0.54	0.85	Homo sapiens matrix metallopeptidase 11 (stromelysin 3) (MMP11), mRNA [NM_005940]
A_23_P259955	NM_000557	GDF5	0.53	0.25	Homo sapiens growth differentiation factor 5 (GDF5), mRNA [NM_000557]
A_23_P211631	NM_006486	FBLN1	0.52	0.23	Homo sapiens fibulin 1 (FBLN1), transcript variant D, mRNA [NM_006486]

3ng/mL TGF- $\beta$ 2					
ProbeID	PrimaryAccession	GeneSymbol	24h	48h	Description
A_33_P3418833	NM_198391	FLRT3	0.51	0.43	Homo sapiens fibronectin leucine rich transmembrane protein 3 (FLRT3), transcript variant 2, mRNA [NM_198391]
A_23_P214168	NM_004370	COL12A1	0.51	0.34	Homo sapiens collagen, type XII, alpha 1 (COL12A1), transcript variant long, mRNA [NM_004370]
A_33_P3294509	NM_000610	CD44	0.51	0.38	Homo sapiens CD44 molecule (Indian blood group) (CD44), transcript variant 1, mRNA [NM_000610]
A_33_P3382856	NM_133507	DCN	0.50	0.21	Homo sapiens decorin (DCN), transcript variant E, mRNA [NM_133507]
A_33_P3238250	NM_016946	F11R	0.50	0.60	Homo sapiens F11 receptor (F11R), mRNA [NM_016946]
A_23_P64873	NM_001920	DCN	0.49	0.19	Homo sapiens decorin (DCN), transcript variant A1, mRNA [NM_001920]
A_33_P3369964	ENST00000569119	ATXN1L	0.49	0.57	ataxin 1-like [Source:HGNC Symbol;Acc:HGNC:33279] [ENST00000569119]
A_23_P99063	NM_002345	LUM	0.49	0.25	Homo sapiens lumican (LUM), mRNA [NM_002345]
A_23_P45365	NM_033380	COL4A5	0.49	0.66	Homo sapiens collagen, type IV, alpha 5 (COL4A5), transcript variant 2, mRNA [NM_033380]
A_33_P3231953	NM_004370	COL12A1	0.49	0.41	Homo sapiens collagen, type XII, alpha 1 (COL12A1), transcript variant long, mRNA [NM_004370]
A_23_P116898	NM_000014	A2M	0.48	0.10	Homo sapiens alpha-2-macroglobulin (A2M), mRNA [NM_000014]
A_23_P71530	NM_002546	TNFRSF11B	0.47	0.59	Homo sapiens tumor necrosis factor receptor superfamily, member 11b (TNFRSF11B), mRNA [NM_002546]
A_23_P116898	NM_000014	A2M	0.47	0.12	Homo sapiens alpha-2-macroglobulin (A2M), mRNA [NM_000014]
A_33_P3380625	NM_001291860	HSPG2	0.47	1.01	Homo sapiens heparan sulfate proteoglycan 2 (HSPG2), transcript variant 1, mRNA [NM_001291860]
A_23_P4662	NM_005178	BCL3	0.46	0.51	Homo sapiens B-cell CLL/lymphoma 3 (BCL3), mRNA [NM_005178]
A_23_P71530	NM_002546	TNFRSF11B	0.46	0.61	Homo sapiens tumor necrosis factor receptor superfamily, member 11b (TNFRSF11B), mRNA [NM_002546]
A_23_P71530	NM_002546	TNFRSF11B	0.46	0.59	Homo sapiens tumor necrosis factor receptor superfamily, member 11b (TNFRSF11B), mRNA [NM_002546]
A_23_P71328	NM_030583	MATN2	0.46	0.26	Homo sapiens matrilin 2 (MATN2), transcript variant 2, mRNA [NM_030583]
A_23_P71530	NM_002546	TNFRSF11B	0.46	0.59	Homo sapiens tumor necrosis factor receptor superfamily, member 11b (TNFRSF11B), mRNA [NM_002546]
A_23_P71530	NM_002546	TNFRSF11B	0.46	0.58	Homo sapiens tumor necrosis factor receptor superfamily, member 11b (TNFRSF11B), mRNA [NM_002546]
A_23_P71530	NM_002546	TNFRSF11B	0.46	0.58	Homo sapiens tumor necrosis factor receptor superfamily, member 11b (TNFRSF11B), mRNA [NM_002546]
A_23_P71530	NM_002546	TNFRSF11B	0.46	0.60	Homo sapiens tumor necrosis factor receptor superfamily, member 11b (TNFRSF11B), mRNA [NM_002546]
A_23_P71530	NM_002546	TNFRSF11B	0.46	0.59	Homo sapiens tumor necrosis factor receptor superfamily, member 11b (TNFRSF11B), mRNA [NM_002546]
A_23_P71530	NM_002546	TNFRSF11B	0.46	0.58	Homo sapiens tumor necrosis factor receptor superfamily, member 11b (TNFRSF11B), mRNA [NM_002546]
A_24_P260443	NM_003248	THBS4	0.45	0.43	Homo sapiens thrombospondin 4 (THBS4), mRNA [NM_003248]
A_23_P300033	NM_006206	PDGFRA	0.45	0.45	Homo sapiens platelet-derived growth factor receptor, alpha polypeptide (PDGFRA), mRNA [NM_006206]
A_24_P300777	NM_001109	ADAM8	0.45	0.55	Homo sapiens ADAM metallopeptidase domain 8 (ADAM8), transcript variant 1, mRNA [NM_001109]
A_24_P150466	NM_001034852	SMOC1	0.44	0.77	Homo sapiens SPARC related modular calcium binding 1 (SMOC1), transcript variant 1, mRNA [NM_001034852]
A_33_P3339531	NM_138481	CHADL	0.44	0.65	Homo sapiens chondroadherin-like (CHADL), mRNA [NM_138481]
A_23_P71530	NM_002546	TNFRSF11B	0.44	0.59	Homo sapiens tumor necrosis factor receptor superfamily, member 11b (TNFRSF11B), mRNA [NM_002546]
A_24_P319364	NM_016946	F11R	0.44	0.45	Homo sapiens F11 receptor (F11R), mRNA [NM_016946]

3ng/mL TGF- $\beta$ 2					
ProbeID	PrimaryAccession	GeneSymbol	24h	48h	Description
A_23_P254741	NM_003102	SOD3	0.43	0.20	Homo sapiens superoxide dismutase 3, extracellular (SOD3), mRNA [NM_003102]
A_23_P116898	NM_000014	A2M	0.43	0.28	Homo sapiens alpha-2-macroglobulin (A2M), mRNA [NM_000014]
A_33_P3381338	NM_019105	TNXB	0.42	0.29	Homo sapiens tenascin XB (TNXB), transcript variant XB, mRNA [NM_019105]
A_23_P153320	NM_000201	ICAM1	0.42	0.50	Homo sapiens intercellular adhesion molecule 1 (ICAM1), mRNA [NM_000201]
A_33_P3363799	NM_001242607	NCAM1	0.42	0.43	Homo sapiens neural cell adhesion molecule 1 (NCAM1), transcript variant 5, mRNA [NM_001242607]
A_23_P153320	NM_000201	ICAM1	0.42	0.48	Homo sapiens intercellular adhesion molecule 1 (ICAM1), mRNA [NM_000201]
A_23_P10121	NM_003012	SFRP1	0.42	0.27	Homo sapiens secreted frizzled-related protein 1 (SFRP1), mRNA [NM_003012]
A_33_P3337485	NM_020404	CD248	0.41	0.54	Homo sapiens CD248 molecule, endosialin (CD248), mRNA [NM_020404]
A_23_P153320	NM_000201	ICAM1	0.41	0.49	Homo sapiens intercellular adhesion molecule 1 (ICAM1), mRNA [NM_000201]
A_23_P153320	NM_000201	ICAM1	0.41	0.48	Homo sapiens intercellular adhesion molecule 1 (ICAM1), mRNA [NM_000201]
A_33_P3299220	NM_025008	ADAMTSL4	0.41	0.31	Homo sapiens ADAMTS-like 4 (ADAMTSL4), transcript variant 2, mRNA [NM_025008]
A_33_P3263432	NM_003637	ITGA10	0.41	0.57	Homo sapiens integrin, alpha 10 (ITGA10), transcript variant 1, mRNA [NM_003637]
A_23_P153320	NM_000201	ICAM1	0.41	0.48	Homo sapiens intercellular adhesion molecule 1 (ICAM1), mRNA [NM_000201]
A_23_P218858	NM_015429	ABI3BP	0.41	0.41	Homo sapiens ABI family, member 3 (NESH) binding protein (ABI3BP), mRNA [NM_015429]
A_23_P69179	NM_018192	P3H2	0.41	0.69	Homo sapiens prolyl 3-hydroxylase 2 (P3H2), transcript variant 1, mRNA [NM_018192]
A_23_P153320	NM_000201	ICAM1	0.41	0.51	Homo sapiens intercellular adhesion molecule 1 (ICAM1), mRNA [NM_000201]
A_23_P153320	NM_000201	ICAM1	0.41	0.50	Homo sapiens intercellular adhesion molecule 1 (ICAM1), mRNA [NM_000201]
A_23_P153320	NM_000201	ICAM1	0.40	0.47	Homo sapiens intercellular adhesion molecule 1 (ICAM1), mRNA [NM_000201]
A_23_P10121	NM_003012	SFRP1	0.40	0.30	Homo sapiens secreted frizzled-related protein 1 (SFRP1), mRNA [NM_003012]
A_23_P10121	NM_003012	SFRP1	0.40	0.24	Homo sapiens secreted frizzled-related protein 1 (SFRP1), mRNA [NM_003012]
A_23_P153320	NM_000201	ICAM1	0.39	0.48	Homo sapiens intercellular adhesion molecule 1 (ICAM1), mRNA [NM_000201]
A_23_P34744	NM_000396	CTSK	0.39	0.24	Homo sapiens cathepsin K (CTSK), mRNA [NM_000396]
A_23_P153320	NM_000201	ICAM1	0.39	0.48	Homo sapiens intercellular adhesion molecule 1 (ICAM1), mRNA [NM_000201]
A_33_P3271156	NM_001204352	SPOCK3	0.39	0.12	Homo sapiens sparc/osteonectin, cwcv and kazal-like domains proteoglycan (testican) 3 (SPOCK3), transcript variant 3, mRNA [NM_001204352]
A_23_P393645	NM_139025	ADAMTS13	0.39	0.53	Homo sapiens ADAM metallopeptidase with thrombospondin type 1 motif, 13 (ADAMTS13), transcript variant 1, mRNA [NM_139025]
A_23_P82868	NM_000930	PLAT	0.39	0.82	Homo sapiens plasminogen activator, tissue (PLAT), transcript variant 1, mRNA [NM_000930]
A_23_P82868	NM_000930	PLAT	0.39	0.84	Homo sapiens plasminogen activator, tissue (PLAT), transcript variant 1, mRNA [NM_000930]
A_23_P82868	NM_000930	PLAT	0.39	0.82	Homo sapiens plasminogen activator, tissue (PLAT), transcript variant 1, mRNA [NM_000930]
A_23_P82868	NM_000930	PLAT	0.39	0.82	Homo sapiens plasminogen activator, tissue (PLAT), transcript variant 1, mRNA [NM_000930]
A_23_P128919	NM_002306	LGALS3	0.38	0.31	Homo sapiens lectin, galactoside-binding, soluble, 3 (LGALS3), transcript variant 1, mRNA [NM_002306]
A_23_P10121	NM_003012	SFRP1	0.38	0.33	Homo sapiens secreted frizzled-related protein 1 (SFRP1), mRNA [NM_003012]

3ng/mL TGF- $\beta$ 2					
ProbeID	PrimaryAccession	GeneSymbol	24h	48h	Description
A_23_P69497	NM_003278	CLEC3B	0.38	0.23	Homo sapiens C-type lectin domain family 3, member B (CLEC3B), mRNA [NM_003278]
A_23_P82868	NM_000930	PLAT	0.38	0.82	Homo sapiens plasminogen activator, tissue (PLAT), transcript variant 1, mRNA [NM_000930]
A_23_P82868	NM_000930	PLAT	0.38	0.83	Homo sapiens plasminogen activator, tissue (PLAT), transcript variant 1, mRNA [NM_000930]
A_23_P82868	NM_000930	PLAT	0.38	0.81	Homo sapiens plasminogen activator, tissue (PLAT), transcript variant 1, mRNA [NM_000930]
A_23_P10121	NM_003012	SFRP1	0.38	0.28	Homo sapiens secreted frizzled-related protein 1 (SFRP1), mRNA [NM_003012]
A_23_P10121	NM_003012	SFRP1	0.38	0.29	Homo sapiens secreted frizzled-related protein 1 (SFRP1), mRNA [NM_003012]
A_23_P82868	NM_000930	PLAT	0.38	0.84	Homo sapiens plasminogen activator, tissue (PLAT), transcript variant 1, mRNA [NM_000930]
A_23_P82868	NM_000930	PLAT	0.38	0.84	Homo sapiens plasminogen activator, tissue (PLAT), transcript variant 1, mRNA [NM_000930]
A_23_P217379	NM_033641	COL4A6	0.38	0.23	Homo sapiens collagen, type IV, alpha 6 (COL4A6), transcript variant B, mRNA [NM_033641]
A_23_P55544	NM_133459	CCBE1	0.38	0.31	Homo sapiens collagen and calcium binding EGF domains 1 (CCBE1), mRNA [NM_133459]
A_23_P82868	NM_000930	PLAT	0.38	0.83	Homo sapiens plasminogen activator, tissue (PLAT), transcript variant 1, mRNA [NM_000930]
A_33_P3308749	NM_001105207	LAMA4	0.37	0.19	Homo sapiens laminin, alpha 4 (LAMA4), transcript variant 3, mRNA [NM_001105207]
A_23_P204630	NM_021229	NTN4	0.37	0.36	Homo sapiens netrin 4 (NTN4), mRNA [NM_021229]
A_23_P386320	NM_033316	MFI2	0.37	0.30	Homo sapiens antigen p97 (melanoma associated) identified by monoclonal antibodies 133.2 and 96.5 (MFI2), transcript variant 2, mRNA [NM_033316]
A_23_P46781	NM_003638	ITGA8	0.36	0.20	Homo sapiens integrin, alpha 8 (ITGA8), transcript variant 1, mRNA [NM_003638]
A_32_P70315	NM_003256	TIMP4	0.36	0.66	Homo sapiens TIMP metallopeptidase inhibitor 4 (TIMP4), mRNA [NM_003256]
A_33_P3377364	NM_000213	ITGB4	0.36	0.27	Homo sapiens integrin, beta 4 (ITGB4), transcript variant 1, mRNA [NM_000213]
A_23_P10121	NM_003012	SFRP1	0.36	0.33	Homo sapiens secreted frizzled-related protein 1 (SFRP1), mRNA [NM_003012]
A_33_P3411975	NM_015429	ABI3BP	0.35	0.50	Homo sapiens ABI family, member 3 (NESH) binding protein (ABI3BP), mRNA [NM_015429]
A_23_P10121	NM_003012	SFRP1	0.33	0.27	Homo sapiens secreted frizzled-related protein 1 (SFRP1), mRNA [NM_003012]
A_32_P80850	NM_021110	COL14A1	0.33	0.23	Homo sapiens collagen, type XIV, alpha 1 (COL14A1), mRNA [NM_021110]
A_23_P134835	NM_018371	CSGALNACT1	0.33	0.23	Homo sapiens chondroitin sulfate N-acetylgalactosaminyltransferase 1 (CSGALNACT1), transcript variant 2, mRNA [NM_018371]
A_23_P134237	NM_002889	RARRES2	0.32	0.21	Homo sapiens retinoic acid receptor responder (tazarotene induced) 2 (RARRES2), mRNA [NM_002889]
A_23_P10121	NM_003012	SFRP1	0.31	0.25	Homo sapiens secreted frizzled-related protein 1 (SFRP1), mRNA [NM_003012]
A_23_P10121	NM_003012	SFRP1	0.31	0.27	Homo sapiens secreted frizzled-related protein 1 (SFRP1), mRNA [NM_003012]
A_23_P308974	NM_207517	ADAMTSL3	0.31	0.22	Homo sapiens ADAMTS-like 3 (ADAMTSL3), transcript variant 1, mRNA [NM_207517]
A_24_P220485	NM_182487	OLFML2A	0.31	0.41	Homo sapiens olfactomedin-like 2A (OLFML2A), transcript variant 1, mRNA [NM_182487]
A_33_P3308744	NM_001105206	LAMA4	0.30	0.19	Homo sapiens laminin, alpha 4 (LAMA4), transcript variant 1, mRNA [NM_001105206]
A_23_P58251	NM_001014448	CPZ	0.30	0.15	Homo sapiens carboxypeptidase Z (CPZ), transcript variant 3, mRNA [NM_001014448]
A_33_P3262560	NR_130106	LAMA3	0.29	0.85	Homo sapiens laminin, alpha 3 (LAMA3), transcript variant 6, non-coding RNA [NR_130106]
A_23_P100660	NM_002615	SERPINF1	0.29	0.17	Homo sapiens serpin peptidase inhibitor, clade F (alpha-2 antiplasmin, pigment epithelium derived factor), member 1 (SERPINF1), mRNA [NM_002615]
A_33_P3391603	NM_001105209	LAMA4	0.27	0.27	Homo sapiens laminin, alpha 4 (LAMA4), transcript variant 5, mRNA [NM_001105209]
A_24_P275073	NM_139155	ADAMTS14	0.26	0.16	Homo sapiens ADAM metallopeptidase with thrombospondin type 1 motif, 14 (ADAMTS14), transcript variant 1, mRNA [NM_139155]

3ng/mL TGF- $\beta$ 2					
ProbeID	PrimaryAccession	GeneSymbol	24h	48h	Description
A_23_P116898	NM_000014	A2M	0.26	0.28	Homo sapiens alpha-2-macroglobulin (A2M), mRNA [NM_000014]
A_23_P200780	NM_003243	TGFBR3	0.24	0.18	Homo sapiens transforming growth factor, beta receptor III (TGFBR3), transcript variant 1, mRNA [NM_003243]
A_23_P134419	NM_007155	ZP3	0.24	1.14	Homo sapiens zona pellucida glycoprotein 3 (sperm receptor) (ZP3), transcript variant 2, mRNA [NM_007155]
A_23_P115011	NM_019032	ADAMTSL4	0.24	0.29	Homo sapiens ADAMTS-like 4 (ADAMTSL4), transcript variant 1, mRNA [NM_019032]
A_33_P3290709	NM_001167890	EGFL6	0.23	0.08	Homo sapiens EGF-like-domain, multiple 6 (EGFL6), transcript variant 2, mRNA [NM_001167890]
A_23_P102611	NM_003881	WISP2	0.23	0.13	Homo sapiens WNT1 inducible signaling pathway protein 2 (WISP2), mRNA [NM_003881]
A_23_P206280	NM_201525	GPR56	0.23	0.26	Homo sapiens G protein-coupled receptor 56 (GPR56), transcript variant 3, mRNA [NM_201525]
A_33_P3287223	NM_001935	DPP4	0.21	0.13	Homo sapiens dipeptidyl-peptidase 4 (DPP4), mRNA [NM_001935]
A_23_P368154	NM_153703	PODN	0.19	0.11	Homo sapiens podocan (PODN), transcript variant 1, mRNA [NM_153703]
A_33_P3218649	NM_001001995	GPM6B	0.19	0.21	Homo sapiens glycoprotein M6B (GPM6B), transcript variant 1, mRNA [NM_001001995]
A_23_P82929	NM_002514	NOV	0.18	0.33	Homo sapiens nephroblastoma overexpressed (NOV), mRNA [NM_002514]
A_23_P378416	NM_001001996	GPM6B	0.18	0.17	Homo sapiens glycoprotein M6B (GPM6B), transcript variant 2, mRNA [NM_001001996]
A_23_P156708	NM_032470	TNXB	0.18	0.14	Homo sapiens tenascin XB (TNXB), transcript variant XB-S, mRNA [NM_032470]
A_23_P89780	NM_198129	LAMA3	0.16	0.17	Homo sapiens laminin, alpha 3 (LAMA3), transcript variant 1, mRNA [NM_198129]
A_23_P56578	NM_053276	VIT	0.16	0.09	Homo sapiens vitrin (VIT), transcript variant 1, mRNA [NM_053276]
A_23_P110266	NM_024574	NDNF	0.14	0.05	Homo sapiens neuron-derived neurotrophic factor (NDNF), mRNA [NM_024574]
A_23_P134601	NM_057168	WNT16	0.13	0.23	Homo sapiens wingless-type MMTV integration site family, member 16 (WNT16), transcript variant 1, mRNA [NM_057168]
A_24_P10137	NM_014059	RGCC	0.13	0.59	Homo sapiens regulator of cell cycle (RGCC), mRNA [NM_014059]
A_21_P0000154	NM_001204358	SPOCK3	0.11	0.43	Homo sapiens sparc/osteonectin, cwcv and kazal-like domains proteoglycan (testican) 3 (SPOCK3), transcript variant 9, mRNA [NM_001204358]
A_23_P216361	NM_021110	COL14A1	0.10	0.03	Homo sapiens collagen, type XIV, alpha 1 (COL14A1), mRNA [NM_021110]
A_33_P3366540	NM_001130518	CSGALNACT1	0.10	0.19	Homo sapiens chondroitin sulfate N-acetylgalactosaminyltransferase 1 (CSGALNACT1), transcript variant 1, mRNA [NM_001130518]
A_23_P1912	NM_207341	ZP1	0.10	0.08	Homo sapiens zona pellucida glycoprotein 1 (sperm receptor) (ZP1), mRNA [NM_207341]
A_23_P138352	NM_004185	WNT2B	0.09	0.10	Homo sapiens wingless-type MMTV integration site family, member 2B (WNT2B), transcript variant WNT-2B1, mRNA [NM_004185]
A_32_P196263	NM_182920	ADAMTS9	0.07	0.16	Homo sapiens ADAM metallopeptidase with thrombospondin type 1 motif, 9 (ADAMTS9), mRNA [NM_182920]
A_23_P31124	NM_030820	COL21A1	0.06	0.04	Homo sapiens collagen, type XXI, alpha 1 (COL21A1), mRNA [NM_030820]

**Table 5. Expression of Src family kinases in microarray analysis**

Src family kinases	Molecular weight	Signal Evaluation	
		control	TGF- $\beta$ 2
Lyn	56 kDa	2	2
Lck	56 kDa	1	1
Hck	59 and 61 kDa	0	1
Fyn	59 kDa	2	2
c-Fgr	56 kDa	2	2
Blk	55 kDa	0	0
c-Yes	60 kDa	2	2
c-Src	60 kDa	2	2

Signal evaluation: 0; transcripts were not detected, 1; signals for transcripts were insufficient, 2; transcripts were detected.

## References

1998. Comparison of glaucomatous progression between untreated patients with normal-tension glaucoma and patients with therapeutically reduced intraocular pressures. Collaborative Normal-Tension Glaucoma Study Group. *Am J Ophthalmol* 126(4):487-497.

Abu-Hassan DW, Li X, Ryan EI, Acott TS, Kelley MJ. 2015. Induced pluripotent stem cells restore function in a human cell loss model of open-angle glaucoma. *Stem Cells* 33(3):751-761.

Acott TS, Kelley MJ. 2008. Extracellular matrix in the trabecular meshwork. *Exp Eye Res* 86(4):543-561.

Agarwal P, Daher AM, Agarwal R. 2015. Aqueous humor TGF-beta2 levels in patients with open-angle glaucoma: A meta-analysis. *Mol Vis* 21:612-620.

Allingham RR, Liu Y, Rhee DJ. 2009. The genetics of primary open-angle glaucoma: a review. *Exp Eye Res* 88(4):837-844.

Alvarado J, Murphy C, Juster R. 1984. Trabecular meshwork cellularity in primary open-angle glaucoma and nonglaucomatous normals. *Ophthalmology* 91(6):564-579.

Babizhayev MA, Brodskaya MW. 1989. Fibronectin detection in drainage outflow system of human eyes in ageing and progression of open-angle glaucoma. *Mech Ageing Dev* 47(2):145-157.

Bourne RRA, Jonas JB, Bron AM, Cicinelli MV, Das A, Flaxman SR, Friedman DS, Keeffe JE, Kempen JH, Leasher J et al. . 2018. Prevalence and causes of vision loss in high-income countries and in Eastern and Central Europe in 2015: magnitude, temporal trends and projections. *Br J Ophthalmol* 102(5):575-585.

Bradley JM, Kelley MJ, Zhu X, Anderssohn AM, Alexander JP, Acott TS. 2001. Effects of mechanical stretching on trabecular matrix metalloproteinases. *Invest Ophthalmol Vis Sci* 42(7):1505-1513.

Bradley JM, Vranka J, Colvis CM, Conger DM, Alexander JP, Fisk AS, Samples JR, Acott TS. 1998. Effect of matrix metalloproteinases activity on outflow in perfused human organ culture. *Invest Ophthalmol Vis Sci* 39(13):2649-58.

Brown MT, Cooper JA. 1996. Regulation, substrates and functions of src. *Biochim Biophys Acta* 1287(2-3):121-149.

Camras CB, Hedman K, Group ULS. 2003. Rate of response to latanoprost or timolol in patients with ocular hypertension or glaucoma. *J Glaucoma* 12(6):466-9.

Carragher NO, Frame MC. 2004. Focal adhesion and actin dynamics: a place where kinases and proteases meet to promote invasion. *Trends Cell Biol* 14(5):241-249.

Cavet ME, Vollmer TR, Harrington KL, VanDerMeid K, Richardson ME. 2015. Regulation of Endothelin-1-Induced Trabecular Meshwork Cell Contractility by Latanoprostene Bunod. *Invest Ophthalmol Vis Sci* 56(6):4108-4116.

Congdon N, O'Colmain B, Klaver CC, Klein R, Muñoz B, Friedman DS, Kempen J, Taylor HR,

Mitchell P, Group EDPR. 2004. Causes and prevalence of visual impairment among adults in the United States. *Arch Ophthalmol* 122(4):477-485.

Cooper JA, Gould KL, Cartwright CA, Hunter T. 1986. Tyr527 is phosphorylated in pp60c-src: implications for regulation. *Science* 231(4744):1431-1434.

Ethier CR, Kamm RD, Palaszewski BA, Johnson MC, Richardson TM. 1986. Calculations of flow resistance in the juxtaglomerular meshwork. *Invest Ophthalmol Vis Sci* 27(12):1741-50.

Filla MS, Dimeo KD, Tong T, Peters DM. 2017. Disruption of fibronectin matrix affects type IV collagen, fibrillin and laminin deposition into extracellular matrix of human trabecular meshwork (HTM) cells. *Exp Eye Res* 165:7-19.

Flaxman SR, Bourne RRA, Resnikoff S, Ackland P, Braithwaite T, Cincinelli MV, Das A, Jonas JB, Keeffe J, Kempen JH, Leasher J, Limburg H, Naidoo K, Pesudovs K, Silvester A, Stevens GA, Tahhan N, Wong TY, Taylor HR, Vision Loss Expert Group of the Global Burden of Disease S. 2017. Global causes of blindness and distance vision impairment 1990-2020: a systematic review and meta-analysis. *Lancet Glob Health* 5(12):e1221-e1234.

Garway-Heath DF, Crabb DP, Bunce C, Lascaratos G, Amalfitano F, Anand N, Azuara-Blanco A, Bourne RR, Broadway DC, Cunliffe IA, Diamond JP, Fraser SG, Ho TA, Martin KR, McNaught AI, Negi A, Patel K, Russell RA, Shah A, Spry PG, Suzuki K, White ET, Wormald RP, Xing W, Zeyen TG. 2015. Latanoprost for open-angle glaucoma (UKGTS): a randomised, multicentre, placebo-controlled trial. *Lancet* 385(9975):1295-1304.

Gerometta R, Kumar S, Shah S, Alvarez L, Candia O, Danias J. 2013. Reduction of steroid-induced intraocular pressure elevation in sheep by tissue plasminogen activator. *Invest Ophthalmol Vis Sci* 54(13):7903-7909.

Gottanka J, Chan D, Eichhorn M, Lutjen-Drecoll E, Ethier CR. 2004. Effects of TGF-beta2 in perfused human eyes. *Invest Ophthalmol Vis Sci* 45(1):153-158.

Ha CH, Bennett AM, Jin ZG. 2008. A novel role of vascular endothelial cadherin in modulating c-Src activation and downstream signaling of vascular endothelial growth factor. *J Biol Chem* 283(11):7261-7270.

Haraguchi M, Border WA, Huang Y, Noble NA. 2001. t-PA promotes glomerular plasmin generation and matrix degradation in experimental glomerulonephritis. *Kidney Int* 59(6):2146-2155.

Harte MT, Hildebrand JD, Burnham MR, Bouton AH, Parsons JT. 1996. p130Cas, a substrate associated with v-Src and v-Crk, localizes to focal adhesions and binds to focal adhesion kinase. *J Biol Chem* 271(23):13649-13655.

Heijl A, Leske MC, Bengtsson B, Hyman L, Bengtsson B, Hussein M, Early Manifest Glaucoma Trial G. 2002. Reduction of intraocular pressure and glaucoma progression: results from the Early Manifest Glaucoma Trial. *Arch Ophthalmol* 120(10):1268-1279.

Heldin CH, Miyazono K, ten Dijke P. 1997. TGF-beta signalling from cell membrane to nucleus through SMAD proteins. *Nature* 390(6659):465-471.

Hill LJ, Mead B, Blanch RJ, Ahmed Z, De Cogan F, Morgan-Warren PJ, Mohamed S, Leadbeater W, Scott RA, Berry M, Logan A. 2015. Decorin Reduces Intraocular Pressure and Retinal Ganglion Cell Loss in Rodents Through Fibrolysis of the Scarred Trabecular Meshwork. *Invest Ophthalmol Vis Sci* 56(6):3743-3757.

Huvaneers S, Danen EH. 2009. Adhesion signaling - crosstalk between integrins, Src and Rho. *J Cell Sci* 122(Pt 8):1059-1069.

Inoue-Mochita M, Inoue T, Fujimoto T, Kameda T, Awai-Kasaoka N, Ohtsu N, Kimoto K, Tanihara H. 2015. p38 MAP kinase inhibitor suppresses transforming growth factor- $\beta$ 2-induced type 1 collagen production in trabecular meshwork cells. *PLoS One* 10(3):e0120774.

Inoue-Mochita M, Inoue T, Kojima S, Futakuchi A, Fujimoto T, Sato-Ohira S, Tsutsumi U, Tanihara H. 2018. Interleukin-6-mediated trans-signaling inhibits transforming growth factor- $\beta$  signaling in trabecular meshwork cells. *J Biol Chem*.

Itoh S, ten Dijke P. 2007. Negative regulation of TGF- $\beta$  receptor/Smad signal transduction. *Curr Opin Cell Biol* 19(2):176-184.

Iwase A, Suzuki Y, Araie M, Yamamoto T, Abe H, Shirato S, Kuwayama Y, Mishima HK, Shimizu H, Tomita G et al. . 2004. The prevalence of primary open-angle glaucoma in Japanese: the Tajimi Study. *Ophthalmology* 111(9):1641-1648.

Izumchenko E, Singh MK, Plotnikova OV, Tikhmyanova N, Little JL, Serebriiskii IG, Seo S, Kurokawa M, Egleston BL, Klein-Szanto A, Pugacheva EN, Hardy RR, Wolfson M, Connolly DC, Golemis EA. 2009. NEDD9 promotes oncogenic signaling in mammary tumor development. *Cancer Res* 69(18):7198-7206.

Johnson M. 2006. 'What controls aqueous humour outflow resistance?'. *Exp Eye Res* 82(4):545-557.

Jove R, Hanafusa H. 1987. Cell transformation by the viral src oncogene. *Annu Rev Cell Biol* 3:31-56.

Kalouche G, Beguier F, Bakria M, Melik-Parsadanian S, Leriche C, Debeir T, Rostène W, Baudouin C, Vigé X. 2016. Activation of Prostaglandin FP and EP2 Receptors Differently Modulates Myofibroblast Transition in a Model of Adult Primary Human Trabecular Meshwork Cells. *Invest Ophthalmol Vis Sci* 57(4):1816-1825.

Kaplan KB, Swedlow JR, Morgan DO, Varmus HE. 1995. c-Src enhances the spreading of src-/- fibroblasts on fibronectin by a kinase-independent mechanism. *Genes Dev* 9(12):1505-1517.

Keller KE, Bhattacharya SK, Borrás T, Brunner TM, Chansangpetch S, Clark AF, Dismuke WM, Du Y, Elliott MH, Ethier CR et al. . 2018. Consensus recommendations for trabecular meshwork cell isolation, characterization and culture. *Exp Eye Res* 171:164-173.

Kersey JP, Broadway DC. 2006. Corticosteroid-induced glaucoma: a review of the literature. *Eye (Lond)* 20(4):407-416.

Kim KS, Lee BH, Kim IS. 1992. The measurement of fibronectin concentrations in human aqueous humor. *Korean J Ophthalmol* 6(1):1-5.

Kirihara T, Shimazaki A, Nakamura M, Miyawaki N. 2014. Ocular hypotensive efficacy of Src-family

tyrosine kinase inhibitors via different cellular actions from Rock inhibitors. *Exp Eye Res* 119:97-105.

Komiya Y, Onodera Y, Kuroiwa M, Nomimura S, Kubo Y, Nam JM, Kajiwara K, Nada S, Oneyama C, Sabe H, Okada M. 2016. The Rho guanine nucleotide exchange factor ARHGEF5 promotes tumor malignancy via epithelial-mesenchymal transition. *Oncogenesis* 5(9):e258.

Kubota R, Kudoh J, Mashima Y, Asakawa S, Minoshima S, Heitmancik JF, Oguchi Y, Shimizu N. 1998. Genomic organization of the human myocilin gene (MYOC) responsible for primary open angle glaucoma (GLC1A). *Biochem Biophys Res Commun* 242(2):396-400.

Kumar S, Shah S, Tang HM, Smith M, Borras T, Danias J. 2013. Tissue plasminogen activator in trabecular meshwork attenuates steroid induced outflow resistance in mice. *PLoS One* 8(8):e72447.

Kypta RM, Goldberg Y, Ulug ET, Courtneidge SA. 1990. Association between the PDGF receptor and members of the src family of tyrosine kinases. *Cell* 62(3):481-492.

Larsson P, Ulfhammar E, Magnusson M, Bergh N, Lunke S, El-Osta A, Medcalf RL, Svensson PA, Karlsson L, Jern S. 2012. Role of histone acetylation in the stimulatory effect of valproic acid on vascular endothelial tissue-type plasminogen activator expression. *PLoS One* 7(2):e31573.

Lee D, Gautschi O. 2006. Clinical development of SRC tyrosine kinase inhibitors in lung cancer. *Clin Lung Cancer* 7(6):381-384.

Lombardo LJ, Lee FY, Chen P, Norris D, Barrish JC, Behnia K, Castaneda S, Cornelius LA, Das J, Doweyko AM, Fairchild C, Hunt JT, Inigo I, Johnston K, Kamath A, Kan D, Klei H, Marathe P, Pang S, Peterson R, Pitt S, Schieven GL, Schmidt RJ, Tokarski J, Wen ML, Wityak J, Borzilleri RM. 2004. Discovery of N-(2-chloro-6-methyl- phenyl)-2-(6-(4-(2-hydroxyethyl)-piperazin-1-yl)-2-methylpyrimidin-4- ylamino)thiazole-5-carboxamide (BMS-354825), a dual Src/Abl kinase inhibitor with potent antitumor activity in preclinical assays. *J Med Chem* 47(27):6658-6661.

Longworth MS, Laimins LA. 2006. Histone deacetylase 3 localizes to the plasma membrane and is a substrate of Src. *Oncogene* 25(32):4495-4500.

Lutjen-Drecoll E, Futa R, Rohen JW. 1981. Ultrahistochemical studies on tangential sections of the trabecular meshwork in normal and glaucomatous eyes. *Invest Ophthalmol Vis Sci* 21(4):563-573.

Lutjen-Drecoll E, Rittig M, Rauterberg J, Jander R, Mollenhauer J. 1989. Immunomicroscopical study of type VI collagen in the trabecular meshwork of normal and glaucomatous eyes. *Exp Eye Res* 48(1):139-147.

Massip Copiz MM, Santa Coloma TA. 2016. c- Src and its role in cystic fibrosis. *Eur J Cell Biol* 95(10):401-413.

Matsuda A, Asada Y, Takakuwa K, Sugita J, Murakami A, Ebihara N. 2015. DNA Methylation Analysis of Human Trabecular Meshwork Cells During Dexamethasone Stimulation. *Invest Ophthalmol Vis Sci* 56(6):3801-3809.

Matsuyama R, Okuzaki D, Okada M, Oneyama C. 2016. MicroRNA-27b suppresses tumor progression by regulating ARFGEF1 and focal adhesion signaling. *Cancer Sci* 107(1):28-35.

Miyazono K. 2009. Transforming growth factor-beta signaling in epithelial-mesenchymal transition and progression of cancer. *Proc Jpn Acad Ser B Phys Biol Sci* 85(8):314-323.

Nada S, Okada M, MacAuley A, Cooper JA, Nakagawa H. 1991. Cloning of a complementary DNA for a protein-tyrosine kinase that specifically phosphorylates a negative regulatory site of p60c-src. *Nature* 351(6321):69-72.

Nada S, Yagi T, Takeda H, Tokunaga T, Nakagawa H, Ikawa Y, Okada M, Aizawa S. 1993. Constitutive activation of Src family kinases in mouse embryos that lack Csk. *Cell* 73(6):1125-1135.

Nakajima E, Nakajima T, Minagawa Y, Shearer TR, Azuma M. 2005. Contribution of ROCK in contraction of trabecular meshwork: proposed mechanism for regulating aqueous outflow in monkey and human eyes. *J Pharm Sci* 94(4):701-708.

Nguyen TD, Chen P, Huang WD, Chen H, Johnson D, Polansky JR. 1998. Gene structure and properties of TIGR, an olfactomedin-related glycoprotein cloned from glucocorticoid-induced trabecular meshwork cells. *J Biol Chem* 273(11):6341-6350.

Ochiai Y, Ochiai H. 2002. Higher concentration of transforming growth factor-beta in aqueous humor of glaucomatous eyes and diabetic eyes. *Jpn J Ophthalmol* 46(3):249-253.

Okada M. 2012. Regulation of the SRC family kinases by Csk. *Int J Biol Sci* 8(10):1385-1397.

Parsons SJ, Parsons JT. 2004. Src family kinases, key regulators of signal transduction. *Oncogene* 23(48):7906-7909.

Pease ME, McKinnon SJ, Quigley HA, Kerrigan-Baumrind LA, Zack DJ. 2000. Obstructed axonal transport of BDNF and its receptor TrkB in experimental glaucoma. *Invest Ophthalmol Vis Sci* 41(3):764-774.

Playford MP, Schaller MD. 2004. The interplay between Src and integrins in normal and tumor biology. *Oncogene* 23(48):7928-7946.

Quigley HA. 2011. Glaucoma. *Lancet* 377(9774):1367-1377.

Quigley HA, Broman AT. 2006. The number of people with glaucoma worldwide in 2010 and 2020. *Br J Ophthalmol* 90(3):262-7.

Quigley HA, McKinnon SJ, Zack DJ, Pease ME, Kerrigan-Baumrind LA, Kerrigan DF, Mitchell RS. 2000. Retrograde axonal transport of BDNF in retinal ganglion cells is blocked by acute IOP elevation in rats. *Invest Ophthalmol Vis Sci* 41(11):3460-6.

Read AT, Chan DW, Ethier CR. 2007. Actin structure in the outflow tract of normal and glaucomatous eyes. *Exp Eye Res* 84(1):214-226.

Roy Chowdhury U, Hann CR, Stamer WD, Fautsch MP. 2015. Aqueous humor outflow: dynamics and disease. *Invest Ophthalmol Vis Sci* 56(5):2993-3003.

Schaller MD. 2001. Paxillin: a focal adhesion-associated adaptor protein. *Oncogene*

20(44):6459-6472.

Seftor RE, Stamer WD, Seftor EA, Snyder RW. 1994. Dexamethasone decreases tissue plasminogen activator activity in trabecular meshwork organ and cell cultures. *J Glaucoma* 3(4):323-328.

Sima N, Cheng X, Ye F, Ma D, Xie X, Lu W. 2013. The overexpression of scaffolding protein NEDD9 promotes migration and invasion in cervical cancer via tyrosine phosphorylated FAK and SRC. *PLoS One* 8(9):e74594.

Tellios N, Belrose JC, Tokarewicz AC, Hutnik C, Liu H, Leask A, Motolko M, Iijima M, Parapuram SK. 2017. TGF- $\beta$  induces phosphorylation of phosphatase and tensin homolog: implications for fibrosis of the trabecular meshwork tissue in glaucoma. *Sci Rep* 7(1):812.

Thomas SM, Brugge JS. 1997. Cellular functions regulated by Src family kinases. *Annu Rev Cell Dev Biol* 13:513-609.

Vranka JA, Kelley MJ, Acott TS, Keller KE. 2015. Extracellular matrix in the trabecular meshwork: intraocular pressure regulation and dysregulation in glaucoma. *Exp Eye Res* 133:112-125.

Wang J, Zhuang S. 2017. Src family kinases in chronic kidney disease. *Am J Physiol Renal Physiol* 313(3):F721-F728.

Wecker T, Han H, Borner J, Grehn F, Schlunck G. 2013. Effects of TGF-beta2 on cadherins and beta-catenin in human trabecular meshwork cells. *Invest Ophthalmol Vis Sci* 54(10):6456-6462.

Wiederholt M, Thieme H, Stumpff F. 2000. The regulation of trabecular meshwork and ciliary muscle contractility. *Prog Retin Eye Res* 19(3):271-295.

Wordinger RJ, Fleenor DL, Hellberg PE, Pang IH, Tovar TO, Zode GS, Fuller JA, Clark AF. 2007. Effects of TGF-beta2, BMP-4, and gremlin in the trabecular meshwork: implications for glaucoma. *Invest Ophthalmol Vis Sci* 48(3):1191-1200.

Yamada M, Hiratsuka Y, Roberts CB, Pezzullo ML, Yates K, Takano S, Miyake K, Taylor HR. 2010. Prevalence of visual impairment in the adult Japanese population by cause and severity and future projections. *Ophthalmic Epidemiol* 17(1):50-57.

Yamamoto T, Iwase A, Araie M, Suzuki Y, Abe H, Shirato S, Kuwayama Y, Mishima HK, Shimizu H, Tomita G et al. . 2005. The Tajimi Study report 2: prevalence of primary angle closure and secondary glaucoma in a Japanese population. *Ophthalmology* 112(10):1661-1669.

Yang Z, Eton D, Zheng F, Livingstone AS, Yu H. 2005. Effect of tissue plasminogen activator on vascular smooth muscle cells. *J Vasc Surg* 42(3):532-538.

Yeatman TJ. 2004. A renaissance for SRC. *Nat Rev Cancer* 4(6):470-480.

Yoneda K, Nakano M, Mori K, Kinoshita S, Tashiro K. 2007. Disease-related quantitation of TGF-beta3 in human aqueous humor. *Growth Factors* 25(3):160-167.

Yu N, Zhang Z, Chen P, Zhong Y, Cai X, Hu H, Yang Y, Zhang J, Li K, Ge J, Yu K, Liu X, Zhuang J. 2015. Tetramethylpyrazine (TMP), an Active Ingredient of Chinese Herb Medicine Chuanxiong, Attenuates the Degeneration of Trabecular Meshwork through SDF-1/CXCR4

Axis. PLoS One 10(8):e0133055.

## Publication

Teruhisa Tsukamoto, Kentaro Kajiwara, Shigeyuki Nada, and Masato Okada

Src mediates TGF- $\beta$ -induced intraocular pressure elevation in glaucoma

Journal of Cellular Physiology, in press, 2018

## Acknowledgments

I would like to express my deepest gratitude to Prof. Masato Okada for his great support, advice, discussion, and encouragement. I am especially grateful to Dr. Shigeyuki Nada and Dr. Kentaro Kajiwara for their helpful advices.

I would like to thank the Core Instrumentation Facility, Research Institute for Microbial Diseases, Osaka University, for technical assistance with LC-MS/MS analysis.

I would like to express my thanks to Prof. Takahisa Furukawa (Osaka University) and Prof. Hiroaki Miki (Osaka University) for reviewing my thesis.

Finally, I am deeply grateful to my family and all members of Department of Research for their encouragement.

This work was supported by JSPS KAKENHI Grant Numbers 15H04296, 26640078, 26114006, 17H06004, and 17K19596.